Multi-Resource Collaborative Service Restoration of a Distribution Network with Decentralized Hierarchical Droop Control

Wei Zhang, Cong Zhang, *Member*, *IEEE*, Jiayong Li, *Member*, *IEEE*, Lipeng Zhu, *Member*, *IEEE*, Shiran Cao, Wen Huang, *Member*, *IEEE*, and Zhikang Shuai, *Senior Member*, *IEEE*

***Abstract*—To improve the resilience of distribution networks (DNs) in the event of extreme natural disasters such as typhoons and rainstorms, it is imperative to efficiently implement distribution service restoration (DSR) to restore loads as soon as possible. In previous studies, DSR has mainly adopted the distributed resource model with droop or PQ control. This inhibits the exploitation of the potential of distributed generators (DGs) in load restoration when the DN loses support from the upstream transmission network. Thus, this paper proposes a multi-resource collaborative service restoration (MRCSR) approach for DNs incorporating local soft open points, DGs, and tie switches. The MRCSR model is developed by integrating a decentralized hierarchical droop control (DHDC) strategy and incorporating the frequency and voltage features of the load demand. A two-stage iterative feedback optimization (TSIFO) algorithm is then developed to analyze the MRCSR model in an accurate and efficient manner. Finally, the proposed model and algorithm are tested on the modified IEEE 33-bus system and a practical distribution system of the Taiwan Power Company to verify their effectiveness and advantages over existing approaches.**

***Index Terms*—Multi-resource collaborative service restoration, distribution network, two-stage iterative feedback, decentralized hierarchical, droop control.**

NOMENCLATURE

DNs	distribution networks
DSR	distribution service restoration
DGs	distributed generators
MRCSR	multi-resource collaborative service restoration
DHDC	decentralized hierarchical droop control
TSIFO	two-stage iterative feedback optimization
SOPs	soft open points
TSs	tie switches
CDC	conventional droop control
MINLP	mixed-integer nonlinear programming
MISOCP	mixed-integer second-order cone programming
$\text{PRO}_{\text{MINLP}}$	MINLP problem
$\text{PRO}_{\text{MISOCP}}$	MISOCP problem
$\text{PRO}_{\text{RMISOCP}}$	$\text{PRO}_{\text{MISOCP}}$ with relaxed integer vector (such as $\boldsymbol{y}$)
$\text{PRO}_{\text{CMISOCP}}$	$\text{PRO}_{\text{MISOCP}}$ with integer vector (such as $\boldsymbol{x}$) removed
TPC	Taiwan Power Company

Received: June 30, 2023
Accepted: October 18, 2023
Published Online: January 1, 2024
Cong Zhang (corresponding author) is with the College of Electrical and Information Engineering, Hunan University, Changsha 410082, China (e-mail: zcong@hnu.edu.cn).
DOI: 10.23919/PCMP.2023.000530

I. INTRODUCTION

In recent years, extreme natural disasters such as storms and floods have occurred frequently around the world because of global warming [1]–[3]. Recent hurricanes such as Harvey, Ida, and Ian have caused severe power outages and economic losses totaling hundreds of millions of dollars. With natural disasters inducing large-scale power outages in bulk power grids, low-voltage distribution networks (DNs) suffer from a high risk of losing power support from the upstream transmission grids [4]. In these circumstances, there are significant power outages in DNs. For DN outage management, distribution service restoration (DSR) is one of the key measures to restore loads as soon as possible during the outage [5]. In general, after the upstream utility grid outage, DSR can be achieved by using multiple heterogeneous resources, such as soft open points (SOPs), distributed generators (DGs), and tie switches (TSs), to restore loads and improve the resilience of the DN, and this has recently attracted widespread attention [6]. However, there are still problems such as low DG utilization and insufficient load restoration capability in the DSR process. Thus, there is an urgent need for developing an efficient DSR approach that allows fast load restoration in the absence of upstream grid support.

There are two main areas of research for the DSR problem: DSR modelling and its solution algorithm. Existing models for DSR can be mainly divided into two categories: those using a single type of resources and

those coordinating multiple types. Single-resource type models for DSR typically employ DGs [7]–[14], TSs [15]–[18], or other local resources [19]–[21]. In [7]–[9], the influence of the DG model on load restoration is discussed in terms of the PQ control and start-up methods, and the optimal size and location of DGs. Reference [10] focuses on the synchronization and circulating currents of the DG during load restoration, while various DGs are exploited to form individual islands for restoring the loads in [11]. The impact of DG uncertainty, such as photovoltaic power generation and wind power, on service restoration is studied in [12]–[14]. In [15]–[18], DSR models with TSs are studied from four perspectives: closed-loop restoration, remote control, action schemes, and heterogeneous types. The concept of multi-intelligent body automation is introduced in [19]–[21] to enhance DN resilience using a single type of resource, such as local intelligent measurement, communication facilities and multi-agent systems.

However, the aforementioned studies only focus on load restoration from the perspective of single-resource type models, ignoring the coordination of resources. Models coordinating multiple types of resources are more conducive to service restoration, because local resources such as DGs and TSs can be reasonably allocated. Recently, a multi-source collaborative service restoration model considering different locations was proposed [22] to achieve optimal resource allocation for load restoration. However, the limited regulation capacity of conventional TSs and the underutilization of the DGs' power output have become obstacles to the improvement of multi-source cooperative service restoration.

As a new type of controllable power electronics, SOPs have recently been introduced to replace traditional TSs [23], [24]. They can accurately perform reactive power compensation at low operating costs, while avoiding the risk of frequent switch operations as well as providing voltage support. Thus, they can enhance load restoration capability. In [25], an islanding model consisting of DGs and SOPs is constructed to facilitate the isolation of fault areas and divide the DN into individual self-sustaining areas. A load restoration model with an SOP and multiple interworking TSs is presented in [26], whereas in [27] a coordinated power supply restoration model for multiple SOPs and TSs is developed. A joint optimization framework for multi-resource service restoration with integrated SOPs is proposed in [28] to achieve better service restoration.

The SOPs used in the above studies all adopt a fault-side Uacθ control mode (equivalent to voltage-frequency control) and a non-fault-side UdcQ control mode (equivalent to PQ control), while the DGs mostly employ PQ control. In previous studies [25]–[29], researchers have assumed either the existence of a slack bus in the network or the DN's connection to the upstream transmission network, so the findings are difficult to apply to a real grid. To solve this problem, a generic three-phase flow model for a DN with no slack bus is proposed in [30]. This includes a droop control model of the DG, the load model, and the three-phase feeder model, whereas a robust droop control model for the DGs and SOPs is developed in [31]. However, all these models adopt conventional droop control (CDC), which is influenced by the output and line impedances, making it difficult to allocate power proportionally and resulting in local power shortages, which affect service restoration. Hierarchical droop control [32] is widely used for secondary power control of DGs, but the strong dependence on communication and the central controller is a major weakness. In [33], decentralized hierarchical control without communication is investigated to perform active frequency restoration of the system, but multi-resource load restoration is not addressed.

To the best of our knowledge, multi-resource modelling with decentralized hierarchical droop control (DHDC) has not been investigated for service restoration. DHDC can allow the rational allocation of multiple types of resources to significantly improve DG utilization and load restoration during a power outage. Hence, for efficient load restoration, it is critical to model multi-resource collaborative service restoration (MRCSR) with DHDC for DNs that have lost support from the upstream transmission network. Moreover, the load demand model plays a crucial role in determining the effectiveness of service restoration in DNs. Common load models include those of constant-power [7], static-voltage characteristic [19], and detailed frequency-voltage characteristic [30], [31]. The constant-power model is less accurate in its representation than that of the static-voltage characteristic and often leads to suboptimal practical service restoration. Although the static-voltage characteristic model generally satisfies the requirements for interconnected service restoration, it is unsuitable for scenarios in which the DNs loses support from the upstream transmission network. In such situations, the voltage and frequency fluctuate significantly, affecting service restoration. In this study a detailed load demand model that considers the actual frequency and voltage characteristics of the load demand is adopted. This comprehensive model provides a more accurate representation of the load behaviour in service restoration.

Solution algorithms for the DSR model can be divided into two main categories: artificial intelligence-based and mathematical programming-based [34]. Artificial intelligence-based algorithms make the rules for their own characteristics to find optimized solutions, in contrast to full analytical techniques. They mainly include expert systems [35], heuristics [36], harmony search [37], and metaheuristic algorithms [38]. In general, these methods exhibit high computational speeds but do not guarantee an optimal solution.

Mathematical programming-based algorithms guarantee the optimal solution by establishing the complete optimization problem and solving it using mixed-integer nonlinear programming (MINLP), mixed-integer linear programming, and mixed-integer second-order cone programming (MISOCP) [7]. MISOCP can formulate the original non-convex problem as a convex optimization problem, significantly reducing the computational burden while obtaining an optimal solution. This has attracted considerable attention in recent years [39], [40]. As the principal techniques of MISOCP, linearization and convex relaxation methods are used to perform convex optimization. This is solved directly by an optimization solver (e.g., GUROBI) via the branch and bound method.

However, there are numerous binary integer variables such as branches and load statuses in the solution process. As the size of the case increases, the number of integer variables increases exponentially. Although satisfactory optimal solutions can be obtained using the aforementioned methods, they often take several hours so do not meet practical engineering requirements. Thus, a two-stage solution approach is proposed in [22] to increase solution efficiency. In Stage I, the post-recovery network topology is determined by a heuristic algorithm, while in Stage II, the power output and load restoration are then determined by removing the topological constraints. However, the heuristic algorithm used in Stage I may affect the accuracy of the solution. Another two-stage solution method is developed in [29], wherein the Stage I proposed in [22] is modified by using relaxed convex optimization to obtain the topology of the network and increase the accuracy of the solution. However, this algorithm may not have high accuracy in solving the MRCSR model with DHDC, for the following two reasons: first, the linear primary voltage of the Q-V droop control model for SOPs and DGs becomes a nonlinear square-root term because of the voltage quadratic term in the power-flow equation after convex optimization. Second, because voltage and frequency are both variables in the load model, the nonlinear voltage term of the load model after convex optimization aggravates the high-level nonlinearization of the MRCSR model. This causes the convex optimization problem after linearization and convex relaxation to be the problem with initial values for the voltage and frequency, and the choice of initial values determines the accuracy of the solution, which is often undesirable.

In this paper, an MRCSR approach for DNs is proposed, one which adopts DHDC as the control model for SOPs and DGs, and introduces a two-stage iterative feedback optimization (TSIFO) algorithm. It can allow efficient system power allocation and service restoration without the slack bus while significantly increasing the accuracy and efficiency of analyzing the model. The present study makes the following contributions:

1) An MRCSR model for DN that integrates SOPs, DGs, and TSs is proposed for improving DG utilization and maximizing the load restoration level. In particular, a novel decentralized hierarchical droop control method is developed for SOPs and DGs to appropriately allocate power from different resources during power outages, and a load demand model is incorporated to account for the practical frequency and voltage features of the load demand. Then, the original intractable MRCSR is converted into a convex optimization problem using conical relaxation, Taylor series approximation, and Big-M methods.

2) A TSIFO algorithm is developed to increase the efficiency and accuracy of analyzing the proposed MRCSR model. The algorithm consists of two stages. In Stage I, an iterative feedback method is used to precisely solve the convex optimization problem in a relaxed manner to obtain the radial topology. In Stage II, the load statuses and the power outputs of the SOPs and DGs are determined by quickly solving the problem with the topological constraints removed.

3) The effectiveness of the proposed MRCSR model is verified by comparisons with other cases for the modified IEEE 33-bus system and a practical distribution system of the Taiwan Power Company (TPC). With regard to both solution accuracy and computational speed, the proposed TSIFO algorithm is compared with a straightforward solution using an off-the-shelf commercial optimizer. This demonstrates that the proposed algorithm outperforms the benchmark approaches. A robustness analysis for different DG active power capacities and load rates indicates the robustness of the MRCSR approach.

The remainder of this paper is organized as follows: Section II describes the problem formulation of MRCSR with DHDC, and in Section III, the TSIFO algorithm for analyzing the proposed model is presented. The numerical simulation is described in Section IV, and conclusions are drawn in Section V.

II. Problem Formulation

In this section, the MRCSR framework is proposed, and the main research idea of the paper is introduced. The formulation of the MRCSR problem is presented in detail. It includes the objective functions of the load restoration and the voltage deviation, as well as the constraints of the radial topology, power flow, operating security, and SOP and DG operation with DHDC.

A. Framework of MRCSR

This study focuses on the situation where extreme events disconnect DNs from the upstream transmission network. Hence, prior to the completion of the repair of the damaged infrastructure, DNs are operated in the islanding mode. During this period, the loads in the DN cannot receive power from upstream generators in the

utility grid. Hence, a multi-resource collaboration of DGs, SOPs, and TSs is necessary for service restoration.

To deal with the low DG utilization and insufficient load restoration capability, a framework of MRCSR for the DN is proposed. This mainly consists of the MRCSR model and the TSIFO algorithm, as shown in Fig. 1. It is seen there that various active and passive resources, e.g., source-side, grid-side, switch-side, and load curtailment, can be optimally managed to meet the different operational requirements for load restoration. It is proposed that the MRCSR model involves a large number of integer variables and nonlinear constraints. To analyze the model efficiency and accurately, the TSIFO algorithm is introduced, allowing the load restoration optimization solution to be obtained via a two-stage algorithm based on the convex optimization of the model.

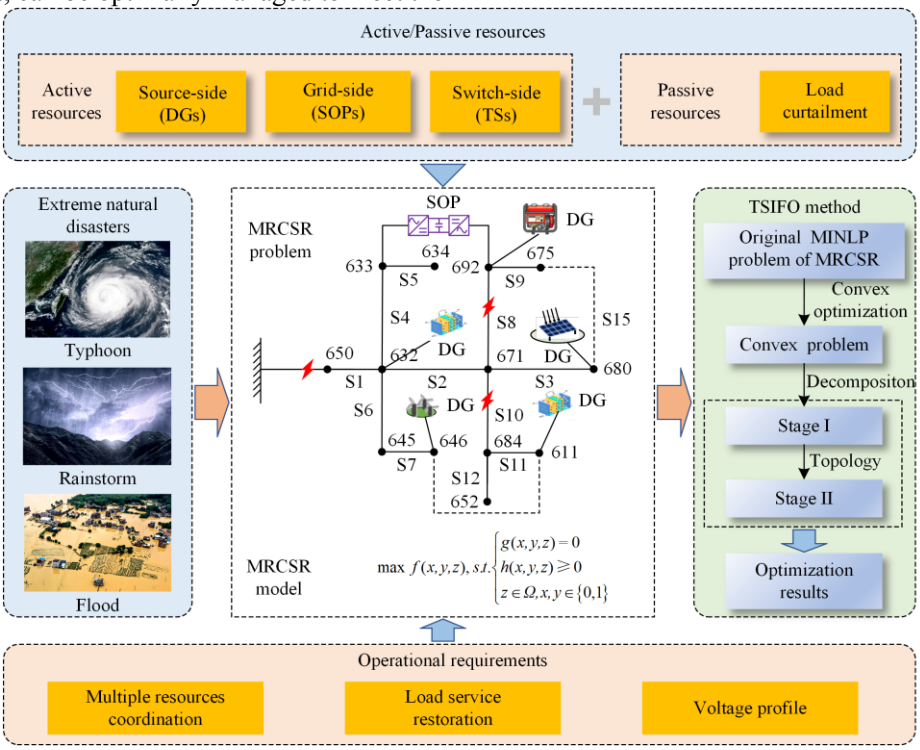

Fig. 1. Framework of MRCSR for the DN.

B. MRCSR Model with the DHDC

1) Objective Function

In the event that the DN loses power support from the upstream transmission network because of an extreme disaster, the MRCSR problem should focus on restoring as many loads as possible. The voltage deviation is an important index for assessing the operational status of the DN [41]. Therefore, the MRCSR objective function is formulated with consideration of both load restoration and voltage deviation mitigation, expressed as:

$$\max f = W_{\mathrm{P}} \sum_{i \in \Omega_{\mathrm{N}}} Y_i P_{\mathrm{L},i} - W_{\mathrm{U}} \Delta M \tag{1}$$

where the first term presents the total load restoration amount and the second term is the sum of the voltage magnitude deviation of all buses; $P_{\mathrm{L},i}$ denotes the aggregate active power load at node i; Y_i is a binary decision variable, with 0 standing for load shedding and 1 for load restoration; W_{P} and W_{U} are the weight coefficients, satisfying $W_{\mathrm{P}} + W_{\mathrm{U}} = 1$, which can be derived by hierarchical analysis to avoid the influence of decision makers on the selection of the weight coefficients as far as possible [41]; and Ω_{N} is a set of nodes of the network. The value of ΔM is chosen according to the following formulation:

$$\Delta M = \sum_{i \in \Omega_{\mathrm{N}}} \left| U_i^2 - \overline{U}^2 \right| = \begin{cases} \sum_{i \in \Omega_{\mathrm{N}}} \left| U_i^2 - (U_{\min}^{\mathrm{de}})^2 \right|, & U_i \leqslant U_{\min}^{\mathrm{de}} \\ 0, & U_{\min}^{\mathrm{de}} \leqslant U_i \leqslant U_{\max}^{\mathrm{de}} \\ \sum_{i \in \Omega_{\mathrm{N}}} \left| U_i^2 - (U_{\max}^{\mathrm{de}})^2 \right|, & U_i \geqslant U_{\max}^{\mathrm{de}} \end{cases} \tag{2}$$

where $U_{\min}^{\mathrm{de}}$ ($U_{\max}^{\mathrm{de}}$) is the desired lower (upper) value of nodal voltage; U_i and $\overline{U}$ represent the voltage amplitude at node i and the auxiliary variable, respectively.

2) Radial Topology Constraints

To describe the radial topology constraints of the distribution network during load restoration, a spanning tree model based on multi-resource collaboration is adopted [22]:

$$\begin{cases} \beta_{ji}+\beta_{ij}=Z_{ji},\ \forall ji\in\Omega_{\mathrm{br}} \\ \sum\limits_{ji\in\Omega_{\mathrm{br}}}\beta_{ji}=1,\ \forall j\in\Omega_{\mathrm{N}}/\Omega_{\mathrm{S}} \\ \sum\limits_{ji\in\Omega_{\mathrm{br}}}\beta_{ji}=0,\ \forall j\in\Omega_{\mathrm{S}} \\ Z_{ji},\beta_{ij},\beta_{ji}\in\{0,1\} \end{cases} \tag{3}$$

where β_{ji} is a binary auxiliary variable that represents whether node *i* is the parent of node *j*; Z_{ji} is a binary variable, and is 1 if the branch *ji* is energized and 0 otherwise; Ω_{br} denotes a set of branches; and Ω_{S} is a set of root nodes with $\Omega_{\mathrm{S}}=1$. The first constraint indicates that if node *i* is the parent of node *j* (i.e., $\beta_{ji}=1$) or node *j* is the parent of node *i* (i.e., $\beta_{ji}=1$), then the branch *ji* is selected to be energized (i.e., Z_{ji}), while β_{ji} and β_{ij} cannot be both 1. The second constraint implies that, except for the root node, each node has exactly one parent node, while the last one means that the root node has no parent node.

3) Power Flow and Security Constraints

A branch flow model [40], which is more suitable for the load-restoration problem, is adopted in this study. The power balance equations are represented by (4) and (5), while the Big-M method is adopted to represent the absence of voltage constraints after branch disconnection and is expressed by (6). The branch capacity constraint is denoted by (7), while constraint (8) represents the detailed load demand model with the effects of frequency and voltage taken into account. The operating safety constraints are (9) and (10).

$$\begin{cases} \sum\limits_{ji\in\Omega_{\mathrm{br}}}(P_{ji}-(I_{ji})^2R_{ji})+P_{\mathrm{in},i}-Y_iP_{\mathrm{L},i}=\sum\limits_{iw\in\Omega_{br}}P_{iw},\ \forall i\in\Omega_{\mathrm{N}} \\ \sum\limits_{ji\in\Omega_{\mathrm{br}}}(Q_{ji}-(I_{ji})^2X_{ji})+Q_{\mathrm{in},i}-Y_iQ_{\mathrm{L},i}=\sum\limits_{iw\in\Omega_{br}}Q_{iw},\ \forall i\in\Omega_{\mathrm{N}} \end{cases} \tag{4}$$

$$\begin{cases} P_{\mathrm{in},i}=P_i^{\mathrm{DG}}+P_i^{\mathrm{SOP}},\ \forall i\in\Omega_{\mathrm{N}} \\ Q_{\mathrm{in},i}=Q_i^{\mathrm{DG}}+Q_i^{\mathrm{SOP}},\ \forall i\in\Omega_{\mathrm{N}} \end{cases} \tag{5}$$

$$\begin{cases} U_j^2\geqslant U_i^2+2(R_{ji}P_{ji}+X_{ji}Q_{ji})-M_1(1-Z_{ji})+ \\ \qquad (R_{ji}^2+X_{ji}^2)I_{ji}^2,\ \forall i,j\in\Omega_{\mathrm{N}} \\ U_j^2\leqslant U_i^2+2(R_{ji}P_{ji}+X_{ji}Q_{ji})+M_1(1-Z_{ji})+ \\ \qquad (R_{ji}^2+X_{ji}^2)I_{ji}^2,\ \forall i,j\in\Omega_{\mathrm{N}} \end{cases} \tag{6}$$

$$P_{ji}^2+Q_{ji}^2=U_j^2I_{ji}^2,\ \forall j\in\Omega_{\mathrm{N}},\forall ji\in\Omega_{\mathrm{br}} \tag{7}$$

$$\begin{cases} P_{\mathrm{L},i}=P_{\mathrm{L},i}^0(k_{\mathrm{pf}}\Delta\omega+1)(U_i)^a,\ \forall i\in\Omega_{\mathrm{N}} \\ Q_{\mathrm{L},i}=Q_{\mathrm{L},i}^0(k_{\mathrm{qf}}\Delta\omega+1)(U_i)^b,\ \forall i\in\Omega_{\mathrm{N}} \\ \Delta\omega=\omega-\omega_0 \end{cases} \tag{8}$$

$$\begin{cases} U_{\min}\leqslant U_j\leqslant U_{\max},\ \forall j\in\Omega_{\mathrm{N}} \\ \omega_{\min}\leqslant\omega\leqslant\omega_{\max} \end{cases} \tag{9}$$

$$\begin{cases} I_{\min}Z_{ji}\leqslant I_{ji}\leqslant I_{\max}Z_{ji},\ \forall ji\in\Omega_{\mathrm{br}} \\ P_{\min}Z_{ji}\leqslant P_{ji}\leqslant P_{\max}Z_{ji},\ \forall ji\in\Omega_{\mathrm{br}} \\ Q_{\min}Z_{ji}\leqslant Q_{ji}\leqslant Q_{\max}Z_{ji},\ \forall ji\in\Omega_{\mathrm{br}} \end{cases} \tag{10}$$

where $P_{ji}(Q_{ji})$ denotes the active (reactive) power of the branch *ji*; $P_{\mathrm{in},i}(Q_{\mathrm{in},i})$ is the active (reactive) power injected at node *i*; $Q_{\mathrm{L},i}$ is the reactive power of the load, while $P_{\mathrm{L},i}^0(Q_{\mathrm{L},i}^0)$ represents the rated active (reactive) power of the load; I_{ji} represents the branch current, while the resistance and reactance are represented by R_{ji} and X_{ji}, respectively; k_{pf} and k_{qf} are constants, whereas a (b) is the active (reactive) power exponent. The corresponding values for different load types can be found in [30]. $\omega(\omega_0)$ stands for the system (reference) frequency; and $\Delta\omega$ is the frequency deviation. The active (reactive) power outputs of DG and SOP at node *i* are represented by $P_i^{\mathrm{DG}}(Q_i^{\mathrm{DG}})$ and $P_i^{\mathrm{SOP}}(Q_i^{\mathrm{SOP}})$, respectively. The lower (upper) values for nodal voltage, system frequency, branch current, branch active and reactive power are represented as $U_{\min}(U_{\max})$, $\omega_{\min}(\omega_{\max})$, $I_{\min}(I_{\max})$, $P_{\min}(P_{\max})$, and $Q_{\min}(Q_{\max})$, respectively. M_1 denotes a positive large number.

4) Operational Constraints Considering the DHDC of SOP and DG

Voltage source converter (VSC) topology is typically adopted for DGs, as shown in Fig. 2. Typically, once the DN loses support from its upstream grid, the micro sources, such as DGs, depend on a peer-to-peer control strategy to maintain the power balance, because there may be no slack bus in the network. The CDC, which mimics the behaviour of synchronous generators through active and reactive power-decoupling control, is commonly used in peer-to-peer control strategies. Using several control loops, such as a current controller, voltage controller, and pulse-width modulation (PWM), the active and reactive power outputs of the VSC as well as the voltage amplitude and frequency can be controlled by the CDC [30], [33], as shown in Fig. 3. With the CDC, the DG reduces the voltage amplitude when reactive power output increases and the frequency when active power output increases. However, as it is affected by both the output and line impedances, the reactive power may not be shared accurately, which in turn may affect the amount of load restoration [32]. In this study, DHDC, which is shown in Figs. 3 and 4, is applied owing to its advantages over centralized and distributed hierarchical control methods, advantages such as its low dependence on communication and good power allocation performance [33]. The main difference between the DHDC and CDC lies in the secondary control items. By measuring the output voltage and global frequency of the local DG, secondary control is used to feed the local

secondary control items $\sigma\omega$ and σU^{DG} back to the DG control unit to enhance the DG's power regulation capability and to maximize load restoration while satisfying constraints such as voltage and frequency. The operational constraints for DHDC of the DG are:

$$0 \leqslant P_j^{\mathrm{DG}} \leqslant P_{j,\max}^{\mathrm{DG}},\ \forall j \in \Omega_{\mathrm{DG}} \tag{11}$$

$$\sqrt{(P_j^{\mathrm{DG}})^2 + (Q_j^{\mathrm{DG}})^2} \leqslant S_j^{\mathrm{DG}},\ \forall j \in \Omega_{\mathrm{DG}} \tag{12}$$

$$\begin{cases} P_j^{\mathrm{DG}} = K_{\mathrm{p}}^{\mathrm{DG}}(\omega_0 - \omega + \sigma\omega),\ \forall j \in \Omega_{\mathrm{DG}} \\ \sigma\omega = K_{\omega}^{\mathrm{DG}}(\omega_0 - \omega) \end{cases} \tag{13}$$

$$\begin{cases} Q_j^{\mathrm{DG}} = K_{\mathrm{q}}^{\mathrm{DG}}(U_0 - U_j + \sigma U^{\mathrm{DG}}),\ \forall j \in \Omega_{\mathrm{DG}} \\ \sigma U^{\mathrm{DG}} = K_{\mathrm{U}}^{\mathrm{DG}}(U_0 - U_{\mathrm{av}}) \end{cases} \tag{14}$$

where $U_0(U_{\mathrm{av}})$ represents the reference (average) voltage magnitude; $\sigma\omega$ and σU^{DG} are the secondary control items of global frequency and voltage; S_j^{DG} and $P_{j,\max}^{\mathrm{DG}}$ are the total and active power output capacities, respectively; $K_{\mathrm{p}}^{\mathrm{DG}}$ and $K_{\mathrm{q}}^{\mathrm{DG}}$ denote the reciprocal of active and reactive droop coefficients, respectively, whereas K_{ω}^{DG} and $K_{\mathrm{U}}^{\mathrm{DG}}$ are the proportional factors of the secondary control items; Ω_{DG} denotes a set of DGs. Active power bound and capacity are represented by (11) and (12), while (13) and (14) are the DHDC expressions for DG.

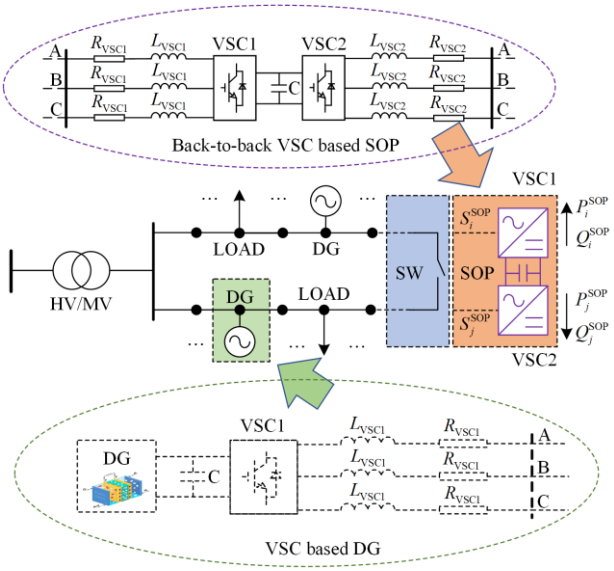

Fig. 2. Topology of DG and SOP.

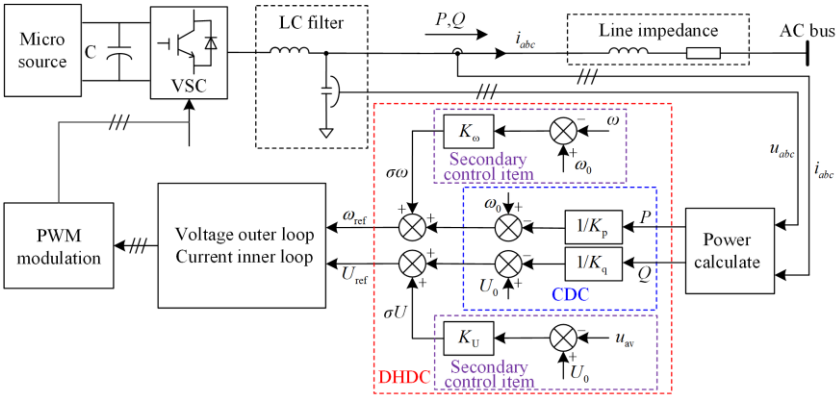

Fig. 3. Schematic diagram of DHDC for micro source.

A common back-to-back VSC [26] is selected for the SOP topological structure, as shown in Fig. 2. It consists of two VSCs coupled with DC capacitors to connect the two AC sides, and allows independent compensation of reactive power at the two AC sides while maintaining control of active power injection. To provide accurate reactive power-sharing support to the system without a slack bus, the DHDC of the SOPs is adopted (Fig. 3) to improve the load restoration capability by feeding the secondary item σU^{SOP} back to the control unit, while the active power control loop remains in PQ control. The specific expressions are given as:

$$P_j^{\mathrm{SOP}} + P_i^{\mathrm{SOP}} + P_j^{\mathrm{SOP,loss}} + P_i^{\mathrm{SOP,loss}} = 0,\ \forall j,i \in \Omega_{\mathrm{SOP}} \tag{15}$$

$$P_j^{\mathrm{SOP,loss}} = A_j^{\mathrm{SOP}} \sqrt{(P_j^{\mathrm{SOP}})^2 + (Q_j^{\mathrm{SOP}})^2},\ \forall j \in \Omega_{\mathrm{SOP}} \tag{16}$$

$$Q_{j,\min}^{\mathrm{SOP}} \leqslant Q_j^{\mathrm{SOP}} \leqslant Q_{j,\max}^{\mathrm{SOP}},\ \forall j \in \Omega_{\mathrm{SOP}} \tag{17}$$

$$\sqrt{(P_j^{\mathrm{SOP}})^2 + (Q_j^{\mathrm{SOP}})^2} \leqslant S_j^{\mathrm{SOP}},\ \forall j \in \Omega_{\mathrm{SOP}} \tag{18}$$

$$\begin{cases} Q_j^{\mathrm{SOP}} = K_{\mathrm{q}}^{\mathrm{SOP}}(U_0 - U_j + \sigma U^{\mathrm{SOP}}),\ \forall j \in \Omega_{\mathrm{SOP}} \\ \sigma U^{\mathrm{SOP}} = K_{\mathrm{U}}^{\mathrm{SOP}}(U_0 - U_{\mathrm{av}}) \end{cases} \tag{19}$$

where σU^{SOP} stands for the secondary control item; S_j^{SOP} denotes the capacity of the SOP; $P_j^{\mathrm{SOP,loss}}$ and A_j^{SOP} are the active power loss and its coefficient, respectively. The lower (upper) reactive power is reflected by $Q_{j,\min}^{\mathrm{SOP}}(Q_{j,\max}^{\mathrm{SOP}})$. $K_{\mathrm{q}}^{\mathrm{SOP}}$ represents the reciprocal of the reactive droop coefficient; $K_{\mathrm{U}}^{\mathrm{SOP}}$ is the proportional factor of the secondary control item; and Ω_{SOP} denotes a set of nodes that connect the SOPs to the network. Active power capacity constraint is represented by (15), and the active power loss is denoted by (16). Reactive power bound and capacity of the SOP are represented by (17) and (18), respectively, while (19) is the DHDC model for SOP.

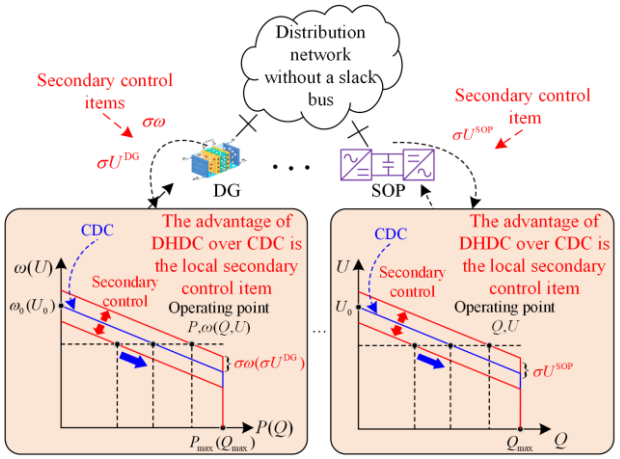

Fig. 4. The DHDC characteristics.

The original MRCSR model in this study consists of (1)–(19). The proposed model includes a large number of integer variables and a set of nonlinear constraints. It is inherently an MINLP problem and is denoted as $\text{PRO}_{\text{MINLP}}$. It is extremely difficult to solve these problems and guarantee the optimality of the solution. To solve the problem, an accurate and fast solution algorithm is proposed in Section III.

III. Solution of MRCSR Model via TSIFO Algorithm

Because the MRCSR model expressed by (1)–(19) in Section II is an MINLP problem, it belongs to the class of NP problems. To solve this problem, a TSIFO algorithm is introduced with the structure shown in Fig. 5. The proposed algorithm consists of a convex optimization method and a TSIFO strategy and procedure. First, the convex optimization method is used to transform the problem into a solvable convex optimization model. The TSIFO strategy and procedure are then developed on this basis to ensure the accuracy and efficiency of the proposed model.

A. Convex Optimization of the MRCSR Model

1) Second-order Conical Relaxation

Because (4) and (6) contain the quadratic terms of branch current and nodal voltage, I_{ji}^{sqr} and U_j^{sqr} are employed to replace the quadratic terms I_{ji}^2 and U_j^2, respectively. The conical formulas can be expressed as:

$$\begin{cases} \sum\limits_{ji\in\Omega_{\text{br}}}(P_{ji}-I_{ji}^{\text{sqr}}R_{ji})+P_{\text{in},i}-Y_iP_{\text{L},i}=\sum\limits_{iw\in\Omega_{\text{br}}}P_{iw},\ \forall i\in\Omega_{\text{N}} \\ \sum\limits_{ji\in\Omega_{\text{br}}}(Q_{ji}-I_{ji}^{\text{sqr}}X_{ji})+Q_{\text{in},i}-Y_iQ_{\text{L},i}=\sum\limits_{iw\in\Omega_{\text{br}}}Q_{iw},\ \forall i\in\Omega_{\text{N}} \end{cases} \tag{20}$$

$$\begin{cases} U_j^{\text{sqr}}\geqslant U_i^{\text{sqr}}+2(R_{ji}P_{ji}+X_{ji}Q_{ji})-M_1(1-Z_{ji})+ \\ \qquad (R_{ji}^2+X_{ji}^2)I_{ji}^{\text{sqr}},\ \forall i,j\in\Omega_{\text{N}} \\ U_j^{\text{sqr}}\leqslant U_i^{\text{sqr}}+2(R_{ji}P_{ji}+X_{ji}Q_{ji})+M_1(1-Z_{ji})+ \\ \qquad (R_{ji}^2+X_{ji}^2)I_{ji}^{\text{sqr}},\ \forall i,j\in\Omega_{\text{N}} \end{cases} \tag{21}$$

The operational constraint of (7), (12), (16), and (18) can be converted into second-order cone expressions as:

$$\left\| \begin{matrix} 2P_{ji} \\ 2Q_{ji} \\ U_j^{\text{sqr}}-I_{ji}^{\text{sqr}} \end{matrix} \right\| \leqslant U_j^{\text{sqr}}+I_{ji}^{\text{sqr}},\ \forall i,j\in\Omega_{\text{N}} \tag{22}$$

$$(P_j^{\text{DG}})^2+(Q_j^{\text{DG}})^2\leqslant 2(S_j^{\text{DG}}/\sqrt{2})(S_j^{\text{DG}}/\sqrt{2}),\ \forall j\in\Omega_{\text{DG}} \tag{23}$$

$$\begin{cases} (P_j^{\text{SOP}})^2+(Q_j^{\text{SOP}})^2\leqslant 2(S_j^{\text{SOP}}/\sqrt{2})(S_j^{\text{SOP}}/\sqrt{2}), \\ \forall j\in\Omega_{\text{SOP}} \\ (P_j^{\text{SOP}})^2+(Q_j^{\text{SOP}})^2\leqslant 2\left(\dfrac{P_j^{\text{SOP,loss}}}{\sqrt{2}A_j^{\text{SOP}}}\right)\left(\dfrac{P_j^{\text{SOP,loss}}}{\sqrt{2}A_j^{\text{SOP}}}\right), \\ \forall j\in\Omega_{\text{SOP}} \end{cases} \tag{24}$$

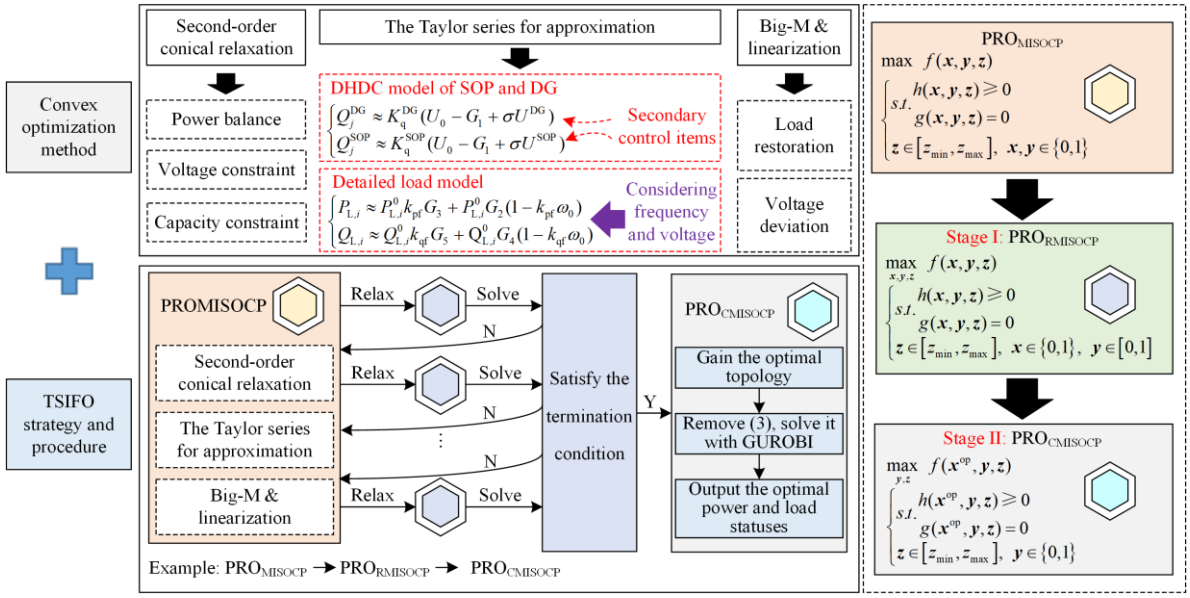

Fig. 5. The structure of the TSIFO algorithm.

2) The Taylor Series for Approximation

The second-order conization of the power-flow equation results in the voltage amplitude U_j in the DHDC expression to be $\sqrt{U_j^{\mathrm{sqr}}}$, causing (14) and (19) to be nonlinear. The following expression can be obtained by applying Taylor series expansion while assuming an initial value $U_{j,k-1}^{\mathrm{str}}$:

$$\sqrt{U_j^{\mathrm{sqr}}} = \frac{1}{2}\sqrt{(U_{j,k-1}^{\mathrm{str}})^2} + \frac{1}{2}\frac{U_j^{\mathrm{sqr}}}{\sqrt{(U_{j,k-1}^{\mathrm{str}})^2}} + \cdots + o(U_j^{\mathrm{sqr}} - (U_{j,k-1}^{\mathrm{str}})^2),\ \forall j \in \Omega_{\mathrm{N}} \tag{25}$$

where $o(\cdot)$ denotes an infinite decimal. Equation (25) can be approximated by neglecting the second and higher-order terms as:

$$U_j = \sqrt{U_j^{\mathrm{sqr}}} \approx \frac{1}{2}U_{j,k-1}^{\mathrm{str}} + \frac{1}{2}\frac{U_j^{\mathrm{sqr}}}{U_{j,k-1}^{\mathrm{str}}} = G_1,\ \forall j \in \Omega_{\mathrm{N}} \tag{26}$$

Then, equations (14) and (19) can be linearly approximated as:

$$\begin{cases} Q_j^{\mathrm{DG}} \approx K_{\mathrm{q}}^{\mathrm{DG}}(U_0 - G_1 + \sigma U^{\mathrm{DG}}),\ \forall j \in \Omega_{\mathrm{DG}} \\ Q_j^{\mathrm{SOP}} \approx K_{\mathrm{q}}^{\mathrm{SOP}}(U_0 - G_1 + \sigma U^{\mathrm{SOP}}),\ \forall j \in \Omega_{\mathrm{SOP}} \end{cases} \tag{27}$$

The expression (8) is rearranged as:

$$\begin{cases} P_{\mathrm{L},i} = P_{\mathrm{L},i}^0 k_{\mathrm{pf}}\omega(U_i)^a + P_{\mathrm{L},i}^0(U_i)^a(1 - k_{\mathrm{pf}}\omega_0),\ \forall i \in \Omega_{\mathrm{N}} \\ Q_{\mathrm{L},i} = Q_{\mathrm{L},i}^0 k_{\mathrm{qf}}\omega(U_i)^b + Q_{\mathrm{L},i}^0(U_i)^b(1 - k_{\mathrm{qf}}\omega_0),\ \forall i \in \Omega_{\mathrm{N}} \end{cases} \tag{28}$$

where the first term includes the product of voltage magnitude exponential power and frequency $\omega(U_i)^a$, while the second term contains exponential power of voltage magnitude $(U_i)^a$, both of which are highly nonlinear. The following linear expressions (29) and (30) are obtained after expanding the second term with Taylor series and given initial values $U_{i,k-1}^{\mathrm{str}}$ and $\omega_{k-1}^{\mathrm{str}}$, while the Taylor series approximation is conducted on the first term [42].

$$\begin{cases} (U_i)^a \approx (U_{i,k-1}^{\mathrm{str}})^a + a(U_{i,k-1}^{\mathrm{str}})^{a-1}(G_1 - U_{i,k-1}^{\mathrm{str}}) + \\ \quad (U_{i,k-1}^{\mathrm{str}})^{a-2}(U_i^{\mathrm{sqr}} - 2G_1U_{i,k-1}^{\mathrm{str}} + (U_{i,k-1}^{\mathrm{str}})^2) = \\ \quad G_2,\ \forall i \in \Omega_{\mathrm{N}} \\ (U_i)^b \approx (U_{i,k-1}^{\mathrm{str}})^b + a(U_{i,k-1}^{\mathrm{str}})^{b-1}(G_1 - U_{i,k-1}^{\mathrm{str}}) + \\ \quad (U_{i,k-1}^{\mathrm{str}})^{b-2}(U_i^{\mathrm{sqr}} - 2G_1U_{i,k-1}^{\mathrm{str}} + (U_{i,k-1}^{\mathrm{str}})^2) = \\ \quad G_4,\ \forall i \in \Omega_{\mathrm{N}} \end{cases} \tag{29}$$

$$\begin{cases} \omega(U_i)^a = -\frac{1}{2}((U_i)^a - \omega)^2 + \frac{1}{2}(((U_i)^a)^2 + (\omega)^2) \approx \\ -\frac{1}{2}(G_2 - \omega)((U_{i,k-1}^{\mathrm{str}})^a - \omega_{k-1}^{\mathrm{str}}) + \frac{1}{2}(G_2(U_{i,k-1}^{\mathrm{str}})^a + \omega\omega_{k-1}^{\mathrm{str}}) = \\ G_3,\ \forall i \in \Omega_{\mathrm{N}} \\ \omega(U_i)^b = -\frac{1}{2}((U_i)^b - \omega)^2 + \frac{1}{2}(((U_i)^b)^2 + (\omega)^2) \approx \\ -\frac{1}{2}(G_4 - \omega)((U_{i,k-1}^{\mathrm{str}})^b - \omega_{k-1}^{\mathrm{str}}) + \frac{1}{2}(G_4(U_{i,k-1}^{\mathrm{str}})^b + \omega\omega_{k-1}^{\mathrm{str}}) = \\ G_5,\ \forall i \in \Omega_{\mathrm{N}} \end{cases} \tag{30}$$

The approximated detailed load demand model is adopted by substituting (29) and (30) into (28), as:

$$\begin{cases} P_{\mathrm{L},i} \approx P_{\mathrm{L},i}^0 k_{\mathrm{pf}} G_3 + P_{\mathrm{L},i}^0 G_2(1 - k_{\mathrm{pf}}\omega_0),\ \forall i \in \Omega_{\mathrm{N}} \\ Q_{\mathrm{L},i} \approx Q_{\mathrm{L},i}^0 k_{\mathrm{qf}} G_5 + \mathrm{Q}_{\mathrm{L},i}^0 G_4(1 - k_{\mathrm{qf}}\omega_0),\ \forall i \in \Omega_{\mathrm{N}} \end{cases} \tag{31}$$

3) The Big-M and Linearization Method

As indicated by (1) and (2), the objective function consists of load restoration and voltage deviation, which are both nonlinear and can be linearized using the new variables $A_i^p = Y_i P_{\mathrm{L},i}$ and $A_i^u = \left|U_i^2 - \overline{U}^2\right|$, respectively. The constraints are obtained by adopting the Big-M and linearization methods for the first and second terms, respectively, expressed as:

$$\begin{cases} 0 \leqslant P_{\mathrm{L},i} - A_i^p \leqslant M_2(1 - Y_i),\ \forall i \in \Omega_{\mathrm{N}} \\ 0 \leqslant A_i^p \leqslant M_2 Y_i,\ \forall i \in \Omega_{\mathrm{N}} \end{cases} \tag{32}$$

$$\begin{cases} U_i^{\mathrm{sqr}} - (U_{\max}^{\mathrm{de}})^2 \leqslant A_i^u,\ \forall i \in \Omega_{\mathrm{N}} \\ -U_i^{\mathrm{sqr}} + (U_{\min}^{\mathrm{de}})^2 \leqslant A_i^u,\ \forall i \in \Omega_{\mathrm{N}} \\ A_i^u \geqslant 0,\ \forall i \in \Omega_{\mathrm{N}} \end{cases} \tag{33}$$

where M_2 denotes a large number. If $Y_i = 1$, the constraints of (32) make $A_i^p = P_{\mathrm{L},i}$, otherwise $A_i^p = 0$.

Through convex optimization, the original problem $\mathrm{PRO_{MINLP}}$ is converted into a computable convex optimization problem $\mathrm{PRO_{MISOCP}}$, whose compact form is given by:

$$\max\ f(\boldsymbol{x}, \boldsymbol{y}, \boldsymbol{z}) \quad s.t. \begin{cases} \boldsymbol{h}(\boldsymbol{x}, \boldsymbol{y}, \boldsymbol{z}) \geqslant 0 \\ \boldsymbol{g}(\boldsymbol{x}, \boldsymbol{y}, \boldsymbol{z}) = 0 \\ \boldsymbol{z} \in [\boldsymbol{z}_{\min}, \boldsymbol{z}_{\max}],\ \boldsymbol{x}, \boldsymbol{y} \in \{0,1\} \end{cases} \tag{34}$$

where $\boldsymbol{x}$ denotes a binary vector of closed and open branches; $\boldsymbol{y}$ represents a binary vector of load statuses; and $\boldsymbol{z}$ is a continuous vector. Inequality constraints, including (9)–(11), (17), (21)–(24), and (32)–(33), and equality constraints, including (3), (5), (13), (15), (20), (27), and (31), are shown by $\boldsymbol{h}$ and $\boldsymbol{g}$, respectively.

B. Strategy and Procedure of TSIFO Algorithm

1) Strategy of TSIFO Algorithm

The TSIFO strategy is proposed to solve the problem $\mathrm{PRO_{MISOCP}}$ by sequentially determining the decision variables of the complex problem in two stages. This can be effective for increasing the accuracy of solving $\mathrm{PRO_{MISOCP}}$ and addressing the problem of insufficient computational performance because of the large numbers of integer variables in $\mathrm{PRO_{MISOCP}}$. The proposed strategy is described below.

Stage I: obtain post-fault topology

This stage provides iterative feedback of the initial values to the optimal values to solve the convex optimization problem after relaxation and to quickly de-

termine the large numbers of integer variables associated with the post-fault topology (i.e., $\boldsymbol{x}^{\mathrm{OP}}$). The problem $\mathrm{PRO_{MISOCP}}$ is relaxed to obtain the problem $\mathrm{PRO_{RMISOCP}}$, whose compact form is given by:

$$\max_{\boldsymbol{x},\boldsymbol{y},\boldsymbol{z}} \ f(\boldsymbol{x},\boldsymbol{y},\boldsymbol{z})$$
$$s.t.\begin{cases} \boldsymbol{h}(\boldsymbol{x},\boldsymbol{y},\boldsymbol{z}) \geqslant 0 \\ \boldsymbol{g}(\boldsymbol{x},\boldsymbol{y},\boldsymbol{z}) = 0 \\ \boldsymbol{z} \in [\boldsymbol{z}_{\min},\boldsymbol{z}_{\max}],\ \boldsymbol{x} \in \{0,1\},\ \boldsymbol{y} \in [0,1] \end{cases} \tag{35}$$

In (35), $\boldsymbol{y}$ is the relaxation vector for the load statuses and is allowed to take on any value of [0, 1]. In addition to the relaxation vector, the problem $\mathrm{PRO_{RMISOCP}}$ has the same objective function and constraints as the original $\mathrm{PRO_{MISOCP}}$. The solution complexity of $\mathrm{PRO_{RMISOCP}}$ is identical to that of the network reconfiguration problem, while that problem is a small-scale integer programming problem involving only the switch action, and can be solved in a short time when an optimization solver such as GUROBI is applied. However, in the process of converting $\mathrm{PRO_{MINLP}}$ into a convex optimization problem, the initial values of $U_{i,k-1}^{\mathrm{str}}$ and $\omega_{k-1}^{\mathrm{str}}$ are assumed. However, because the hypothetical values differ significantly from the optimized values, larger computational errors may be introduced in (27) and (31), resulting in $\mathrm{PRO_{MINLP}}$ not being accurately expressed by $\mathrm{PRO_{MISOCP}}$. To achieve an accurate topology-optimized solution, the design of the iterative feedback algorithm for the problem $\mathrm{PRO_{RMISOCP}}$ after relaxation is critical. The solution process is shown in the red dashed box in Fig. 6.

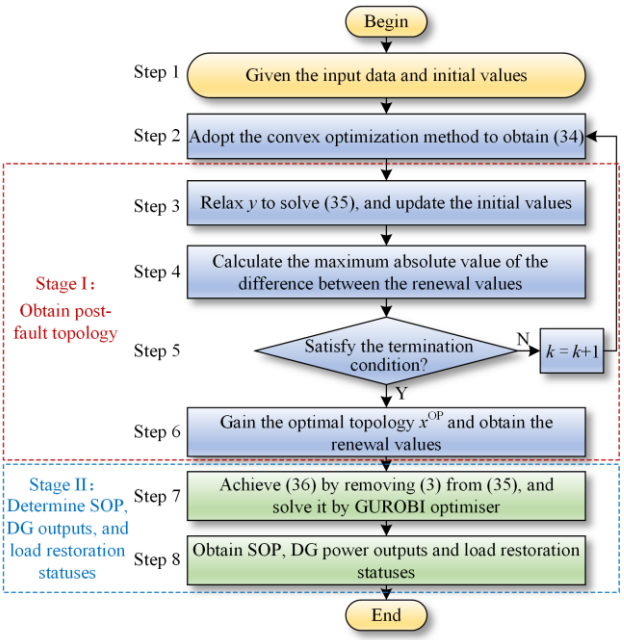

Fig. 6. Flowchart of TSIFO algorithm.

Stage II: determine SOP, DG power outputs, and load restoration statuses

Once the post-fault topology is determined, the topology constraint (3) can be deleted from the problem $\mathrm{PRO_{MISOCP}}$ to form the small-scale problem $\mathrm{PRO_{CMISOCP}}$. Its compact form is given by (36), which can avoid a large number of integer variable operations related to switch-on and switch-off of branches. Thus, the SOPs, DGs power outputs, and load restoration statuses can be quickly identified:

$$\max_{\boldsymbol{y},\boldsymbol{z}} \ f(\boldsymbol{x}^{\mathrm{op}},\boldsymbol{y},\boldsymbol{z})$$
$$s.t.\begin{cases} \boldsymbol{h}(\boldsymbol{x}^{\mathrm{op}},\boldsymbol{y},\boldsymbol{z}) \geqslant 0 \\ \boldsymbol{g}(\boldsymbol{x}^{\mathrm{op}},\boldsymbol{y},\boldsymbol{z}) = 0 \\ \boldsymbol{z} \in [\boldsymbol{z}_{\min},\boldsymbol{z}_{\max}],\ \boldsymbol{y} \in \{0,1\} \end{cases} \tag{36}$$

where $\boldsymbol{x}^{\mathrm{OP}}$ denotes the optimal topology obtained in Stage I.

2) Procedure of TSIFO Algorithm

The procedure of the TSIFO algorithm, which consists of eight steps, is shown in Fig. 6. Step 1 assigns the initial values $U_{i,k-1}^{\mathrm{str}}$, $\omega_{k-1}^{\mathrm{str}}$ and $\Delta_{\max}$ for the iterative feedback, and initializes the iteration index as $k=1$. There is a loop in the algorithm, which starts with Step 2 and ends with Step 6, employing the iterative feedback method to solve (35). In particular, Step 3 is to update the initial values of Stage I by solving $\mathrm{PRO_{RMISOCP}}$. Then, in Step 4, the absolute maximum value $\Delta_{\max}$ of the difference before and after the renewal values is calculated. If the condition of Step 5 is satisfied, the optimal initial values $\sqrt{U_{i,\mathrm{op}}^{\mathrm{sqr}}}$ and ω_{op} are achieved in Step 6, and the post-fault topology is acquired in Stage I. Otherwise, the algorithm returns to Step 2 and continues the above process. Subsequently, equation (36) is achieved by removing (3) from (35). Finally, the SOPs, DGs power outputs, and load restoration statuses are determined rapidly in Step 8 using the optimization solver, and the algorithm terminates. Pseudocode for the above procedure is presented as Algorithm 1.

Algorithm 1: solving MRCSR model with TSIFO

Input data and set $U_{i,k-1}^{\mathrm{str}}$, $\omega_{k-1}^{\mathrm{str}}$, $\Delta_{\max}$, k and ς;
while $\Delta_{\max} > \varsigma$ do
  Solve (35) to obtain U_i^{sqr} and ω;
  Update the value of $U_{i,k}^{\mathrm{str}}$ and ω_k^{str} as
  $U_{i,k}^{\mathrm{str}} = \max(\sqrt{U_i^{\mathrm{sqr}}})$, $\omega_k^{\mathrm{str}} = \omega$;
  Calculate $\Delta_{\max} = \max\left\{\left|U_{i,k}^{\mathrm{str}} - U_{i,k-1}^{\mathrm{str}}\right|, \left|\omega_k^{\mathrm{str}} - \omega_{k-1}^{\mathrm{str}}\right|\right\}$;
  Let $k = k+1$;
end
Obtain the accurate initial values $U_{i,k}^{\mathrm{str}} = \sqrt{U_{i,\mathrm{op}}^{\mathrm{sqr}}}$, $\omega_k^{\mathrm{str}} = \omega_{\mathrm{op}}$, and acquire the post-fault topology vector $\boldsymbol{x}^{\mathrm{op}}$;
Solve (36) to obtain the optimal value of $\boldsymbol{y}$ and $\boldsymbol{z}$;
Output optimal values $\boldsymbol{y}$ and $\boldsymbol{z}$;
end

3) Feasibility of TSIFO Algorithm

In the realm of distribution-network service restoration, there are relevant applications that involve the utilization of two-stage algorithms. In [22], a two-stage algorithm is used to determine feasible restoration paths and formulate recovery strategies for critical loads. Similarly, in [29], a hardening strategy is proposed for distribution systems to withstand natural disasters. The strategy involves a first stage that focuses on the proper scheduling of post-disaster repairs, and is followed by a second stage that involves the judicious selection of components for hardening.

Notably, these studies focus on complex MINLP problems. Using a two-stage algorithm, a computationally intricate optimisation problem is deconstructed into two simpler problems that can be solved sequentially. Thus, the algorithm significantly reduces the computational complexity of large-scale DSR problems.

The TSIFO algorithm is similar to the aforementioned two-stage algorithm. In Stage I, an iterative feedback-based relaxed convex optimization problem is applied to determine a reasonable post-fault radial topology, while the total restored load is approximated as a continuous variable, representing a linear combination of load restoration and shedding. This approximation can be seen as a network reconfiguration problem, ultimately resulting in a relatively optimal outcome for load restoration. However, loads typically exist in one of two statuses: operational or shedding. Consequently, the first stage yields an infeasible solution. To address this, in the absence of topological constraints, Stage II optimizes load statuses and multiple resource power outputs to achieve feasible restoration strategies, including SOPs, DGs outputs, and load restoration statuses. Therefore, the TSIFO algorithm effectively approximates the optimal solution of $\text{PRO}_{\text{MISOCP}}$ [22], [29], confirming the feasibility of the proposed algorithm.

IV. Case Study

In this section, the proposed MRCSR approach is tested on the modified IEEE 33-bus system and a practical distribution system of TPC [7] to validate its effectiveness. Specifically, this consists of verification of the MRCSR model, performance analysis of the TSIFO algorithm and robustness analysis of the MRCSR approach. It is assumed that there are remotely controllable switches on each branch in the system, switches which are automatically executed during service restoration.

A. Tests on the Modified IEEE 33-bus System

The single-line diagram of the modified IEEE33-bus system is shown in Fig. 7. The voltage level of the system is 12.66 kV and the total rated active and reactive power loads are 3.72 MW and 2.30 Mvar, respectively. Detailed load demand data and line parameters can be found in [7].

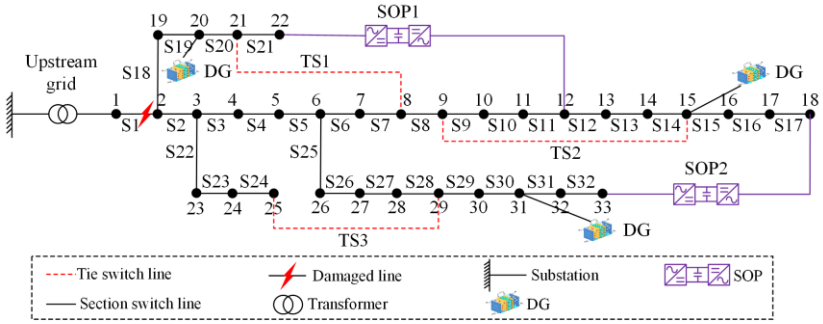

Fig. 7. Single-line diagram of the modified IEEE33-bus system.

The system is modified by integrating three DGs into the DN at buses 15, 20, and 31. The system has 35 branches, including 32 sectionalized branches indicated by the solid lines and 3 tie branches indicated by the dashed lines. The sectionalizing switches and TSs are depicted as 'S' and 'TS' with numbers, respectively. Two TSs, one between buses 12 and 22 and the other between buses 18 and 33, are replaced with SOPs. Table I presents the relevant parameters for the modelling and solving algorithm of the system.

The proposed approach is implemented in the YALMIP optimization toolbox using MATLAB R2021a with the GUROBI optimizer. The experimental environment is a computer running Windows 10 with an Intel(R) i7-6500U CPU @ 2.50 GHz and 8.00 GB RAM.

TABLE I
THE RELEVANT PARAMETERS FOR THE MODEL AND ALGORITHM

Parameters	Value	Parameters	Value
W_P/W_U	0.67/0.33	U_0/ω_0	1.05/1.004 p.u.
A_j^{SOP}/ς	0.02/1e−3	$P_{j,\max}^{DG}$	1.00 MW
$Q_{j,\min}^{SOP}/Q_{j,\max}^{SOP}$	−0.3/0.3 Mvar	S_j^{SOP}/S_j^{DG}	0.45/1.00 MVA
$K_p^{DG}/K_q^{DG}/K_q^{SOP}$	1.25/0.1/0.01	M_1/M_2	0.2/100
$U_{\min}^{de}/U_{\max}^{de}$	0.99/1.01 p.u.	K_{pf}/K_{qf}	1/−1
$U_{\min}/U_{\max}$	0.95/1.05 p.u.	a/b	1.5/1.5
$P_{\max}/Q_{\max}$	1.1 MW/1.1 Mvar	$I_{\min}/I_{\max}$	−0.33/0.33 p.u.
$\omega_{\min}/\omega_{\max}$	0.996/1.004 p.u.	$U_{i,k-1}^{str}/\omega_{k-1}^{str}$	1.0 p.u.
K_ω^{DG}	3.3	K_U^{DG}/K_U^{SOP}	−0.54/5.4

Without loss of generality, it is assumed that an extreme natural disaster causes line S1 to open because of fault isolation. This will result in the DN losing power supply from the upstream transmission network. Three comparative studies are conducted to evaluate the effectiveness of the proposed MRCSR approach. In the first study, the proposed model is validated by comparing it with recently reported methods, whereas in the second study, the performance of the TSIFO algorithm is analyzed to ensure its accuracy and speed. In the last study, an analysis is performed to investigate the robustness of service restoration for different DG active power capacities and load rates.

1) Validity Verification of the MRCSR Model

To validate the effectiveness of the proposed approach, four cases, including those of [30] and [31], are examined.

Case 1: CDC is applied to the DSR model without TS1–TS3, SOP1, and SOP2 [30].

Case 2: CDC is applied to the DSR model with SOP1 and SOP2 but not TS1–TS3 [31].

Case 3: CDC is applied to the DSR model with SOP1 and SOP2 as well as TS1–TS3.

Case 4: DHDC is applied to the MRCSR model with SOP1 and SOP2 as well as TS1–TS3 (the proposed approach).

The load restoration results for the four cases are presented in Table II, while Table III, and Figs. 8 and 9 present the output power of the DGs and SOPs. As is shown, the active power output of the DGs is the main factor limiting the quality of service restoration as well as the reactive power. Distinct from Case 1, Case 2 uses SOPs for load restoration. Reactive power compensation of 176.3 kvar is provided to the DN, which increases the reactive power output of the DGs from 1222.9 kvar to 1269.2 kvar and the active power output from 2585.8 kW to 2749.8 kW. At this time, the load restoration reached 2700 kW, and the load restoration rate is increased by 4%, demonstrating the advantages of SOPs for improving service restoration. Compared with Case 2, Case 3 adds the reconfiguration element, as shown in Fig. 10(a). The active power output of the DGs is not significantly increased, but the load restoration is improved by 20 kW by optimizing the power flow of the system.

In Case 4, the MRCSR model with DHDC is used to rationalize the reactive and active outputs of multiple types of resources by making full use of local measurement information (i.e., nodal voltage and system frequency), performing network reconfiguration, and allowing multiple DGs and SOPs in the system to share the load in a collaborative manner. Therefore, the active power of the DGs is significantly improved, with 99.7% active utilization of DGs, while the reactive power demand required for service restoration is mainly supported by SOPs at 1187.1 kvar. In this case, the load restoration is increased from 2720 kW to 2940 kW, with a load restoration rate of 78.5%, representing a 4.7% increase compared with Case 3. The load restoration results for Case 4 are shown in Fig. 10(b).

TABLE II
LOAD RESTORATION RESULTS FOR FOUR CASES

Results	Load shedding points	Load restoration (kW)	Load restoration rate (%)
Case 1	2–4, 19, 23, 25, 30, 33	2550	68.6
Case 2	2–4, 19, 25, 30	2700	72.6
Case 3	11, 15, 24, 27–28, 30–31	2720	73.2
Case 4	**6, 24, 27–28, 30**	**2940**	**78.5**

TABLE III
OUTPUT OF DGS AND SOPS IN FOUR CASES

Results	Case 1	Case 2	Case 3	**Case 4**
Active power output of DGs (kW)	2585.8	2749.8	2753.9	**2989.3**
Active power utilization rate of DGs (%)	86.2	91.7	91.8	**99.7**
Reactive power output of DGs (kvar)	1222.9	1269.2	1282.0	**302.0**
Reactive power output of SOPs (kvar)		176.3	176.1	**1187.1**

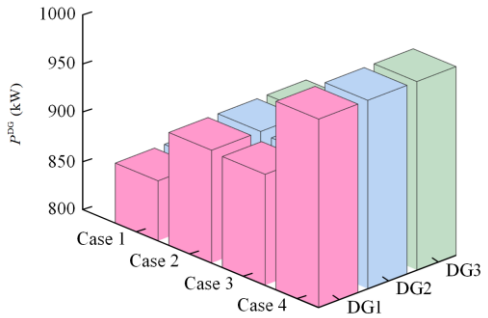

Fig. 8. Active power output of three DGs in four cases.

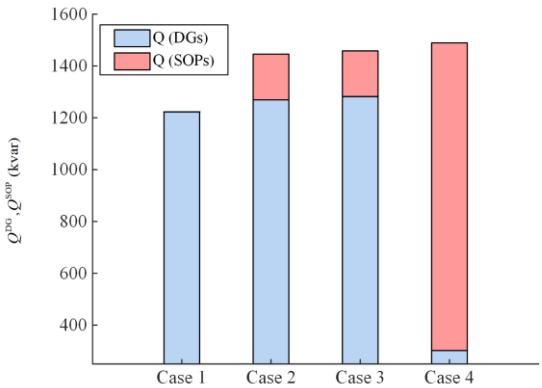

Fig. 9. Reactive power output of DGs and SOPs in four cases.

2) Performance Analysis of TSIFO Algorithm

The accuracy and efficiency of the TSIFO algorithm are evaluated by applying different solution algorithms to different scenarios. To compare the performances of the algorithms, two scenarios are designed: Scenario 1 involves the MRCSR model with TSs but no SOPs, and Scenario 2 involves the proposed model. The two scenarios are implemented using the GUROBI optimizer and the proposed TSIFO algorithm, respectively. Solutions with calculation times of >1 h are regarded as

infeasible (denoted as 'Inf'). The analysis results are presented in Table IV, in which the average results from running the simulation 50 times are shown. The accuracy of the proposed approach is indicated by the relaxation errors of the branch currents [43]. The relaxation deviations of the branch current in different scenarios for the GUROBI optimizer and the proposed approach are shown in Fig. 11.

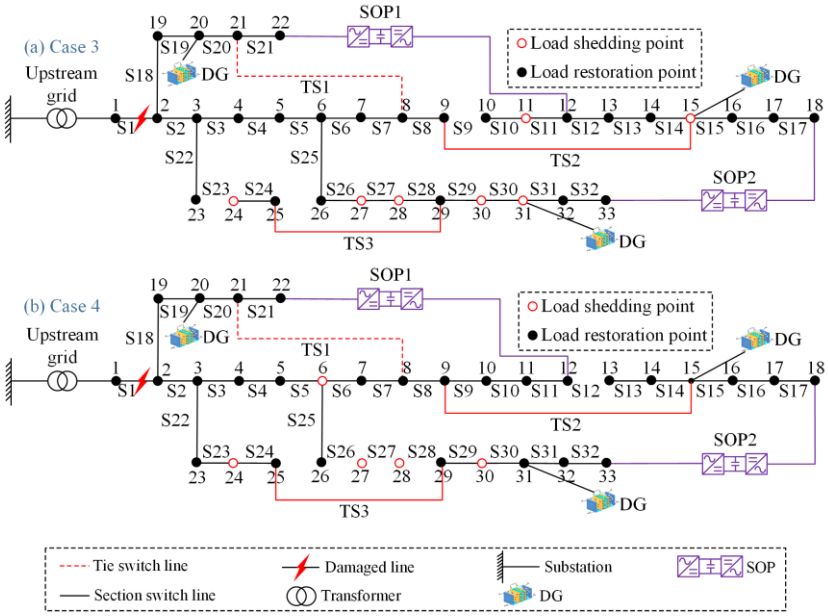

Fig. 10. Load restoration results in Case 3 and Case 4.

TABLE IV
RESULTS OF COMPARATIVE ANALYSIS UNDER THE GUROBI AND TSIFO ALGORITHMS

Results			Scenario 1	Scenario 2
The modified IEEE33-bus system	Load restoration (MW)	GUROBI	2.68	Inf
		TSIFO	2.67	**2.94**
	Computing time (s)	GUROBI	18.50	Inf
		TSIFO	5.64	**7.56**

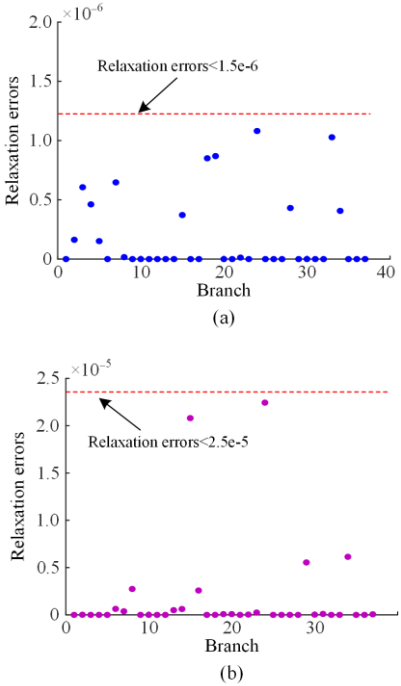

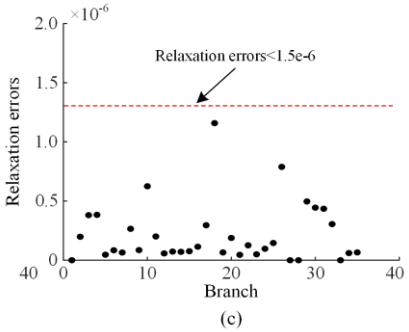

Fig. 11. Scatter plots of relaxation errors for different scenarios. (a) Scenario 1 (GUROBI). (b) Scenario 1 (TSIFO). (c) Scenario 2 (TSIFO).

As indicated in Table IV, the direct application of the GUROBI optimizer solution only provides feasible solutions in Scenario 1. By solving the original MRCSR problem directly, optimal results are obtained. These can be used as the benchmark for the TSIFO algorithm. However, for Scenario 2, there is still no feasible solution after 1 h, mainly owing to the excessive numbers of integer variables. In contrast, both scenarios are successfully solved by the TSIFO algorithm, indicating that the TSIFO algorithm is effective. In Scenario 1, satisfactory results are obtained by the TSIFO algorithm, and are similar to the load restoration results obtained with GUROBI. Compared with the direct GUROBI optimizer, the TSIFO algorithm has a significantly shorter solution time, and its computational speed is 3.2 times faster. This indicates that the proposed algorithm can effectively accelerate the model solution process.

Meanwhile, the relaxation errors for both scenarios under the modified IEEE 33-bus system are small, with the maximum error being less than 2.5e-5, as shown in Fig. 11. Hence, the relaxation of the proposed approach is accurate, and satisfies practical engineering requirements [7].

3) Robustness Analysis of MRCSR Approach

A robustness analysis of the service restoration is conducted for the active power capacity and load demand factor of the DGs. First, the load restoration of the proposed approach is analyzed with respect to the active power capacity of the DGs in the range of 700–1000 kW (step size of 50 kW). The load restoration and the total active power output of the DGs at different DG active power capacities are shown in Fig. 12 and Table V. The reactive power outputs of the DGs and SOPs are shown in Fig. 13. As seen there, when the active power capacity of the DGs increases but is below 850 kW, the active power output of the DGs for all four cases exhibited an upward trend, with corresponding growth in the load restoration.

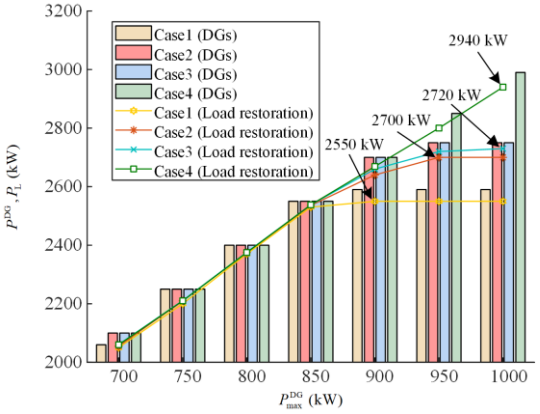

Fig. 12. Load restoration at different active power capacities of DGs.

TABLE V
TOTAL ACTIVE POWER OUTPUT OF DGS AT DIFFERENT ACTIVE POWER CAPACITIES OF DGS

Active power capacity of DGs (kW)	Total active power output (kW)			
	Case 1	Case 2	Case 3	Case 4
700	2059.4	2078.4	2100	**2100**
750	2250	2245.6	2250	**2250**
800	2400	2400	2400	**2400**
850	2550	2550	2550	**2550**
900	2585.8	2700	2700	**2700**
950	2585.8	2749.5	2753.9	**2850**
1000	2585.8	2749.8	2753.9	**2989.3**

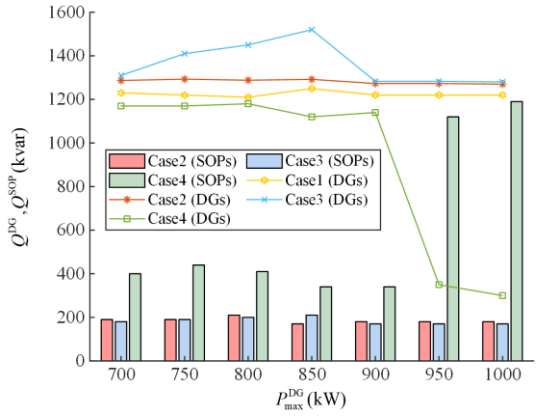

Fig. 13. Total reactive power output of DGs and SOPs at different active power capacity of DGs.

When the active power capacity of the DGs reaches 850 kW, different characteristics emerge. For Case 1, because the active power output of the DGs is close to the capacity of the DGs (so there is no reactive power compensation), the reactive power output of the DGs remains constant, and the load restoration is limited to 2550 kW. The reactive power demand is partially supplied by SOPs in Case 2. This increases the service restoration to 2700 kW. Compared with Case 1, there is an increase of 150 kW, but the CDC does not reasonably allocate the reactive power output, including that of the SOPs, resulting in an unsustainable increase in load restoration. Compared with Case 2, the load restoration in Case 3 is increased by 20 kW, mainly because of the optimized power-flow distribution. In Case 4, the active power utilization of the DGs is significantly improved, and a recovered load of 2940 kW is achieved at the active power capacity of 1000 kW. This is achieved by allocating the reactive power from multiple types of resources so that the majority of the reactive power demand for the restored load comes from the SOPs. Among the methods, the proposed approach achieves the best load restoration performance with different active power capacities of DGs.

Without loss of generality, the load restoration is analyzed at different load rates (0.6, 0.8, 1.0, and 1.2), as shown in Table VI. As seen, the load restoration rate decreases as the load rate increases. A comparison of the four cases reveals that the best load restoration is achieved in Case 4, and in particular, at the load rate of 1.2, with increases of 5.1%, 4.4%, and 4.3% compared to Cases 1, 2 and 3, respectively.

TABLE VI
LOAD RESTORATION AT DIFFERENT LOAD RATES

Load rates	Restored load (kW) and restoration percentage			
	Case 1	Case 2	Case 3	Case 4
60%	1980 (88.7%)	2120 (94.9%)	2240 (100%)	**2250 (100%)**
80%	2310 (77.4%)	2400 (80.7%)	2720 (91.4%)	**2830 (94.6%)**
100%	2550 (68.6%)	2700 (72.6%)	2720 (73.2%)	**2940 (78.5%)**
120%	2690 (60.3%)	2720 (61.0%)	2730 (61.1%)	**2950 (65.4%)**

B. The Practical Distribution System of TPC

A TPC 83-bus system is a practical distribution system, as shown in Fig. 14. The voltage level and reference power of the system are 11.4 kV and 100 MVA,

respectively. The rated capacity of the DG is 0.6 MVA. From the parameters presented in Table I, the rated active power and reactive power are scaled down proportionally to 2.84 MW and 2.07 Mvar, respectively. The relevant modifications are as follows: 11 feeders are connected to the upstream grid via bus 1 and four DGs integrated into the DN at buses 8, 13, 56 and 62. The system has 93 branches, including 82 sectionalized branches indicated by the solid lines and 11 tie branches indicated by the dashed lines. The tie switches are depicted as 'TS' with numbers. Two TSs, one between buses 5 and 55 and the other between buses 20 and 83, are replaced by SOPs. Without loss of generality, it is assumed that the TPC 83-bus system loses support from the upstream transmission network because of an extreme natural disaster. Two scenarios are examined to validate the proposed approach.

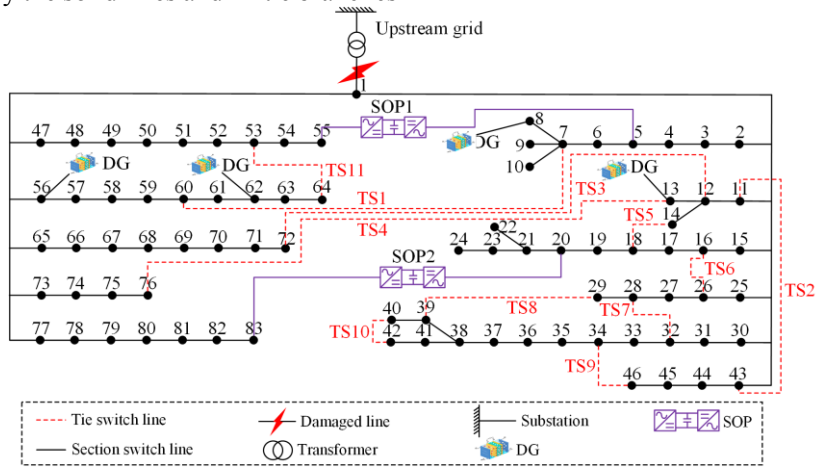

Fig. 14. Topology of the practical 83-bus distribution network of TPC.

Scenario 1: DHDC is applied to the MRCSR model with TS1–TS11 but not SOP1 and SOP2.

Scenario 2: DHDC is applied to the MRCSR model with SOP1 and SOP2 as well as TS1–TS11 (the proposed approach).

The optimization results for the two scenarios are presented in Table VII. The active and reactive power outputs of the DGs and SOPs are shown in Figs. 15 and 16, respectively. In Scenario 2, the SOPs can provide crucial reactive power support, which increases the active power utilization rate of the DGs from 75.2% to 90.0%. Consequently, the load restoration performance in Scenario 2 is superior to that in Scenario 1, reaching 2042 kW. The load restoration results for Scenario 2 are shown in Fig. 17, validating the effectiveness of the proposed model for large-scale practical distribution systems.

TABLE VII
OPTIMIZATION RESULTS FOR TWO SCENARIOS

Results	Scenario 1	Scenario 2
Load restoration (kW)	1800	**2042**
Load restoration rate (%)	63.7	**72.1**
Active power output of DGs (kW)	1805	**2157**
Active power utilization rate of DGs (%)	75.2	**90.0**
Reactive power output of DGs (kvar)	1264.5	**967.0**
Reactive power output of SOPs (kvar)		**875.7**

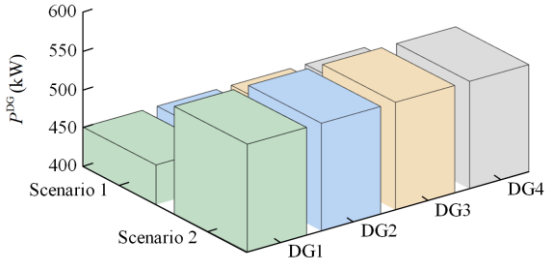

Fig. 15. Active power output of four DGs in two scenarios.

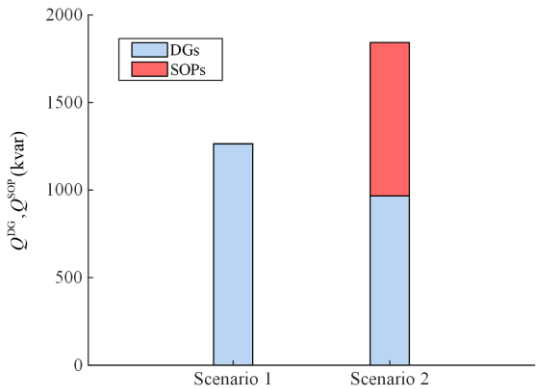

Fig. 16. Reactive power output of DGs and SOPs in two scenarios.

TABLE VIII
RESULTS OF COMPARATIVE ANALYSIS UNDER THE GUROBI AND TSIFO ALGORITHMS

Results			Scenario 1	Scenario 2
The practical distribution system of TPC	Load restoration (MW)	GUROBI	1.82	Inf
		TSIFO	1.80	**2.04**
	Computing time (s)	GUROBI	82.69	Inf
		TSIFO	23.61	**24.68**

The results obtained using the GUROBI and TSIFO algorithms are presented in Table VIII. As shown there,

the computation times increase for both algorithms. However, it remains within a reasonable range [7]. Moreover, the application of the TSIFO algorithm made it easier to achieve satisfactory load restoration outcomes. Figure 18 shows relaxation errors for different scenarios, with the maximum error being less than 1.6e-4. This satisfies the requirements for large-scale practical distribution systems.

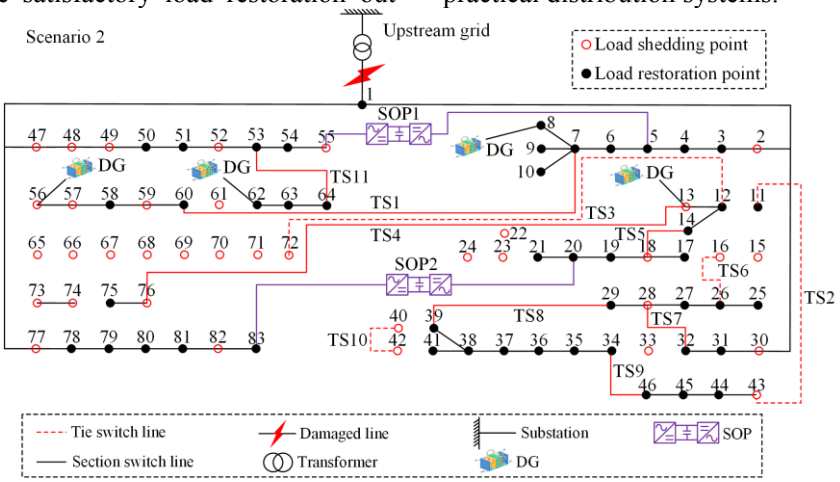

Fig. 17. Load restoration results in Scenario 2.

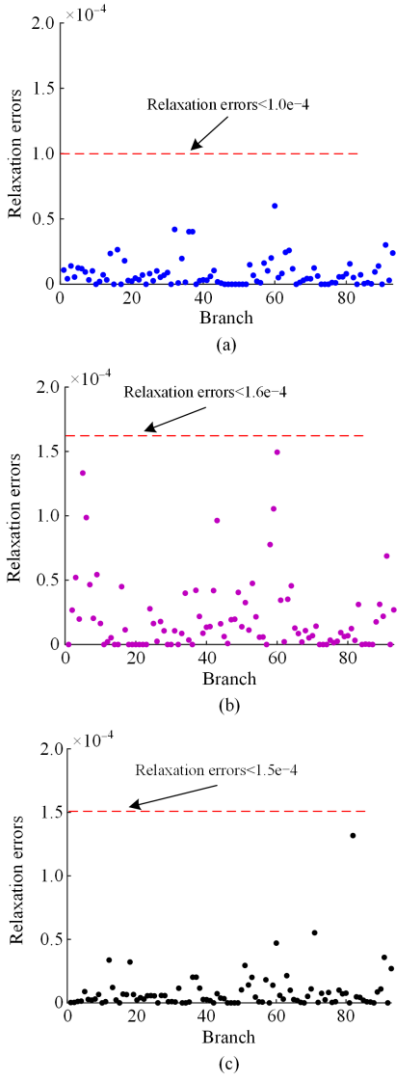

Fig. 18. Scatter plots of relaxation errors for different scenarios. (a) Scenario 1 (GUROBI). (b) Scenario 1 (TSIFO). (c) Scenario 2 (TSIFO).

Figure 19 and Table IX present the load restoration and total power outputs of DGs and SOPs at different DG active power capacities, respectively. As the active power output of DG increases, it gradually approaches its maximum capacity. Although both scenarios adopted the DHDC, the active and reactive power demands of the loads in Scenario 1 are not fully satisfied, leading to a load restoration of only 1800 kW. In contrast, the proposed approach leverages the SOP to provide reactive power support, resulting in a remarkable improvement in DG utilization throughout the incremental process. Consequently, the load restoration keeps increasing until it reaches 2042 kW. Load restoration at different load rates is shown in Table X. As seen, the best load restoration is achieved in Scenario 2.

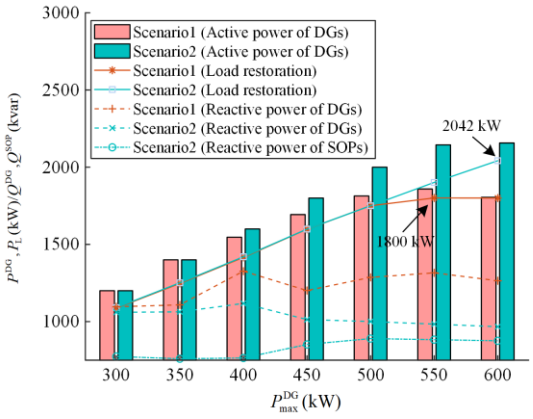

Fig. 19. Load restoration and total power output of DGs and SOPs at different active power capacities of DGs.

From the above analysis, the proposed MRCSR approach has potential for the multi-resource collaborative service restoration of large-scale practical distribution networks when the DN loses support from the upstream transmission network.

TABLE IX
TOTAL ACTIVE POWER OUTPUT OF DGS AT DIFFERENT ACTIVE POWER CAPACITIES OF DGS

Active power capacity of DGs (kW)	Total active power output (kW)	
	Scenario 1	Scenario 2
300	1200	**1200**
350	1400	**1400**
400	1546	**1600**
450	1693	**1800**
500	1814	**2000**
550	1859	**2144**
600	1805	**2157**

TABLE X
LOAD RESTORATION AT DIFFERENT LOAD RATES

Load rates	Restored load (kW) and restoration percentage	
	Scenario 1	Scenario 2
60%	1572 (92.6%)	**1703 (100%)**
80%	1688 (74.6%)	**1966 (86.9%)**
100%	1800 (63.7%)	**2042 (72.1%)**
120%	1847 (54.3%)	**2050 (60.4%)**

V. CONCLUSION

To improve DG utilization and maximize load restoration capability, an MRCSR approach for a DN that integrates SOPs, DGs, and TSs is proposed. The MRCSR model and the TSIFO algorithm are developed. In the proposed model, the DHDC method for SOPs and DGs is used to appropriately allocate power from different sources during outages, and the detailed load demand model is incorporated to illustrate the actual frequency and voltage characteristics of the load demand. To efficiently analyze the proposed model, the TSIFO algorithm is used to obtain the post-fault topology, multi-source outputs, and load restoration status by modelling Stage I as a $\text{PRO}_{\text{RMISOCP}}$ problem and Stage II as a $\text{PRO}_{\text{CMISOCP}}$ problem.

The results reveal that the proposed MRCSR model can significantly increase the DG utilization level and the load restoration rate compared with the benchmark methods, through the DHDC method, the reactive power compensation provided by the SOP, network reconfiguration and detailed load demand model. In addition, the proposed algorithm is more than 3 times faster than the conventional optimizer, and the order of magnitude of the maximum relaxation error is about 10^{-4}, which satisfies practical engineering requirements for fast and accurate service restoration.

ACKNOWLEDGMENT

Not applicable.

AUTHOR'S CONTRIBUTIONS

Wei Zhang: constructed the conceptualization and methodology of multi-resource collaborative service restoration, and was responsible for drafting the original manuscript. Cong Zhang: analyzed the data and contributed to writing the original draft of the manuscript. Jiayong Li: contributed to writing the original draft of the manuscript. Lipeng Zhu: investigated the background of collaborative service restoration and revised English expression. Shiran Cao: performed case studies and validated the rationality of the results. Wen Huang: checked and revised English expression. Zhikang Shuai: was in charge of project management. All authors read and approved the final manuscript.

FUNDING

This work is jointly supported by the National Natural Science Foundation of China (No. 52007056, No. 52207094, and No. 52377095), the Science and Technology Innovation Program of Hunan Province (No. 2023RC3114), and the Key Research and Development Program of Hunan Province (No. 2021SK2051).

AVAILABILITY OF DATA AND MATERIALS

Please contact the corresponding author for data material request.

DECLARATIONS

Competing interests: The authors declare that they have no known competing financial interests or personal relationships that could have appeared to influence the work reported in this paper.

AUTHORS' INFORMATION

Wei Zhang received the B.S. degree in electrical and information engineering from the Hubei University of Technology and the M.S. degree in electrical engineering from Wuhan University, Wuhan, China, respectively. From 2013 to 2017, he worked as a Work Leader at Changde Power Supply Company of State Grid. He was with the Hubei University of Science and Technology as a lecturer from 2017 to 2020. He is currently working toward the Ph.D. degree in electrical engineering at the College of Electrical and Information Engineering, Hunan University, Changsha. His research interests include emergency power and resilient distribution systems.

Cong Zhang received the B.S. degree in mathematics from the school of mathematics in South China University of Technology, Guangzhou, China, in 2013. After that, he began to research electrical engineering, and he is currently an associate professor with the College of Electrical and Information Engineering, Hunan University, Changsha, China. His research interests include reactive power optimization, incorporating uncertainties, and interval power flow analysis.

Jiayong Li received the B.Eng. degree from Zhejiang University, Hangzhou, China, in 2014, and the Ph.D. degree from The Hong Kong Polytechnic University, Hong Kong, in 2018. He is currently an associate professor with the College of Electrical and Information Engineering of Hunan University, Changsha, China. He was a postdoctoral fellow with the Department of Electrical and Computer Engineering, Southern Methodist University from 2019 to 2020, and was a visiting scholar with Argonne National Laboratory in 2017. His research interests include distribution system planning and operation, power economics, demand-side energy management, and distributed control.

Lipeng Zhu received the B.S. degree in electrical engineering from the Huazhong University of Science and Technology, Wuhan, China, in 2012, the M.S. degree in electrical engineering from Wuhan University, Wuhan, China, in 2015, and the Ph.D. degree in electrical engineering from Tsinghua University, Beijing, China, in 2018. He was a postdoctoral fellow/senior research assistant with The University of Hong Kong, Hong Kong, from 2018 to 2021. He is currently a Professor with Hunan University, Changsha, China. His research interests mainly include spatialtemporal energy data analysis, IoT data management and analytics in smart grids, synchrophasor measurement technologies, and data-driven power system stability and control.

Shiran Cao received the B.S. degree from the Changsha University of Science & Technology, Changsha, China, in 2015, the M.S. degree from Hebei University of Technology, Tianjin, China, in 2019. He is currently working toward the Ph.D. degree in electrical engineering with the College of Electrical and Information Engineering, Hunan University, Changsha, China. His major research interests include renewable energy generation, energy storage technology, and vulnerability assessment of microgrids.

Wen Huang received the B.S. and Ph.D. degrees in electrical engineering from Hunan University, Changsha, China, in 2014 and 2020 respectively. During 2018–2020, he was a visiting scholar with the Department of Electrical and Computer Engineering, Illinois Institute of Technology, Chicago, IL, USA. He is currently an associate professor with the College of Electrical and Information Engineering, Hunan University, Changsha, China. His research interests include renewable energy, fault analysis, and control of converters.

Zhikang Shuai received the B.S. and Ph.D. degrees in electrical engineering from the College of Electrical and Information Engineering, Hunan University, Changsha, China, in 2005 and 2011, respectively. He was with Hunan University, as an assistant professor between 2009 and 2012, an associate professor in 2013, and a Professor in 2014. His research interests include power quality control, power electronics, and microgrid stability analysis and control. He is an associate editor for the CSEE Journal of Power and Energy Systems, Chinese Journal of Electrical Engineering. He was the recipient of the 2010 National Scientific and Technological awards of China, the 2012 Hunan Technological Invention awards of China, and the 2007 Scientific and Technological awards from the National Mechanical Industry Association of China.

REFERENCES

[1] M. Groll, "Can climate change be avoided? Vision of a hydrogen-electricity energy economy," *Energy*, vol. 264, Nov. 2022.

[2] J. Li, D. Xu, and J. Wang *et al*., "P2P multigrade energy trading for heterogeneous distributed energy resources and flexible demand," *IEEE Transactions on Smart Grid*, vol. 14, no. 2, pp. 1577-1589, Mar. 2023.

[3] Y. Li, S. He, and Y. Li *et al*., "Probabilistic charging power forecast of EVCS: reinforcement learning assisted deep learning approach," *IEEE Transactions on Intelligent Vehicles*, vol. 8, no. 1, pp. 344-357, Jan. 2023.

[4] C. Chen, J. Wang, and F. Qiu *et al*., "Resilient distribution system by microgrids formation after natural disasters," *IEEE Transactions on Smart Grid*, vol. 7, no. 2, pp. 958-966, Mar. 2016.

[5] J. Li, M. E. Khodayar, and M. R. Feizi, "Hybrid modeling based co-optimization of crew dispatch and distribution system restoration considering multiple uncertainties," *IEEE Systems Journal*, vol. 16, no. 1, pp. 1278-1288, Jan. 2022.

[6] A. Zidan and E. F. El-Saadany, "A cooperative multiagent framework for self-healing mechanisms in distribution systems," *IEEE Transactions on Smart Grid*, vol. 3, no. 3, pp. 1525-1539, Sep. 2012.

[7] Y. Li, J. Xiao, and C. Chen *et al*., "Service restoration model with mixed-integer second-order cone programming for DN with distributed generations," *IEEE Transactions on Smart Grid*, vol. 10, no. 4, pp. 4138-4150, Jul. 2019.

[8] H. Sekhavatmanesh and R. Cherkaoui, "A multi-step reconfiguration model for active DN restoration integrating DG start-up sequences," *IEEE Transactions on Sustainable Energy*, vol. 11, no. 4, pp. 2879-2888, Oct. 2020.

[9] V. Kumar, H. C. R. Kumar, and I. Gupta *et al*., "DG integrated approach for service restoration under cold load pickup," *IEEE Transactions on Power Delivery*, vol. 25, no. 1, pp. 398-406, Jan. 2010.

[10] Y. Xu, C. Liu, and Z. Wang *et al*., "DGs for service restoration to critical loads in a secondary network," *IEEE Transactions on Smart Grid*, vol. 10, no. 1, pp. 435-447, Jan. 2019.

[11] A. Sharma, D. Srinivasan, and A. Trivedi, "A decentralized multiagent system approach for service restoration using DG islanding," *IEEE Transactions on Smart Grid*, vol. 6, no. 6, pp. 2784-2793, Nov. 2015.

[12] W. Liu, and F. Ding, "Collaborative distribution system restoration planning and real-time dispatch considering

behind-the-meter DERs," *IEEE Transactions on Power Systems*,vol. 36, no. 4, pp. 3629-3644, Jul. 2021.

[13] C. Zhang, Q. Liu, and B. Zhou, "A central limit theorem-based method for DC and AC power flow analysis under interval uncertainty of renewable power generation," *IEEE Transactions on Sustainable Energy*, vol. 14, no. 1, pp. 563-575, Jan. 2023.

[14] X. Fu, "Statistical machine learning model for capacitor planning considering uncertainties in photovoltaic power," *Protection and Control of Modern Power Systems*, vol. 7, no. 1, pp. 51-63, Jan. 2022.

[15] A. Arif, B. Cui, and Z. Wang, "Switching device-cognizant sequential distribution system restoration," *IEEE Transactions on Power Systems*, vol. 37, no. 1, pp. 317-329, Jan. 2022.

[16] J. B. Leite, R. A. V. Peralta, and J. R. S. Mantovani, "Restoration switching analysis in the integrated architecture for DN operation," *Electric Power Systems Research*, 2021.

[17] R. Vargas, L. H. Macedo, and J. M. Home-Ortiz *et al*., "Optimal restoration of distribution systems considering transemporary closed-loop operation," *IEEE Systems Journal*, vol. 15, no. 4, pp. 5483-5494, Dec. 2021.

[18] Y. Xu, C. Liu, and K. P. Schneider, "Placement of remote-controlled switches to enhance distribution system restoration capability," *IEEE Transactions on Power Systems*, vol. 31, no. 2, pp. 1139-1150, Mar. 2016.

[19] R. Vargas, L. H. Macedo, and J. M. Home-Ortiz *et al*., "Optimal restoration of active distribution systems with voltage control and closed-loop operation," *IEEE Transactions on Smart Grid*, vol. 12, no. 3, pp. 2295-2306, May 2021.

[20] H. Sekhavatmanesh and R. Cherkaoui, "DN restoration in a multiagent framework using a convex OPF model," *IEEE Transactions on Smart Grid*, vol. 10, no. 3, pp. 2618-2628, Sep. 2019.

[21] Y. Li, S. He, and Y. Li *et al*., "Federated multiagent deep reinforcement learning approach via physics-informed reward for multimicrogrid energy management," *IEEE Transactions on Neural Networks and Learning Systems*, Early Access, pp. 1-13. Jan. 2022.

[22] Y. Wang, Y. Xu, and J. He *et al*., "Coordinating multiple sources for service restoration to enhance resilience of distribution systems," *IEEE Transactions on Smart Grid*, vol. 10, no. 5, pp. 5781-5793, Sep. 2019.

[23] M. Deakin, I. Sarantakos, and D. Greenwood *et al*., "Comparative analysis of services from soft open points using cost–benefit analysis," *Applied Energy*, vol. 333, Mar. 2023.

[24] J. Wang, N. Zhou, and C. Y. Chung *et al*., "Coordinated planning of converter-based DG units and soft open points incorporating active management in unbalanced DNs," *IEEE Transactions on Sustainable Energy*, vol. 11, no. 3, pp. 2015-2027, Jul. 2020.

[25] H. Ji, C. Wang, and P. Li *et al*., "SOP-based islanding partition method of active DNs considering the characteristics of DG, energy storage system and load," *Energy*, vol. 155, pp. 312-325, Jan. 2018.

[26] P. Li, G. Song, and H. Ji, "A supply restoration method of distribution system based on soft open point," in *2016 IEEE Innovative Smart Grid Technologies - Asia (ISGT-Asia)*, Melbourne, Australia, Dec. 2016, pp. 535-539.

[27] P. Li, J. Ji, and H. Ji et al., "Self-healing oriented supply restoration method based on the coordination of multiple SOPs in active DNs," *Energy*, vol. 195, Mar. 2020.

[28] X. Yang, Z. Zhou, and Y. Zhang *et al*., "Resilience-oriented co-deployment of remote-controlled switches and soft open points in DNs," *IEEE Transactions on Power Systems*, vol. 38, no. 2, pp. 1350-1365, Mar. 2023.

[29] Y. Tan, A. K. Das, and P. Arabshahi *et al*., "Distribution systems hardening against natural disasters," *IEEE Transactions on Power Systems*, vol. 33, no. 6, pp. 6849-6860, Sep. 2018.

[30] M. A. Allam, A. A. Hamad, and M. Kazerani, "A generic modeling and power-flow analysis approach for isochronous and droop-controlled microgrids," *IEEE Transactions on Power Systems*, vol. 33, no. 5, pp. 5657-5670, Sep. 2018.

[31] F. Sun, M. Yu, and Q. Wu *et al*., "A multi-time scale energy management method for active DNs with multiple terminal soft open point," *International Journal of Electrical Power and Energy Systems*, 2021.

[32] R. Xu, C. Zhang, and Y. Xu *et al*., "Multi-objective hierarchically-coordinated volt/var control for active DNs with droop-controlled PV inverters," *IEEE Transactions on Smart Grid*, vol. 13, no. 2, pp. 998-1011. Mar. 2022.

[33] J. M. Rey, P. Marti, and M. Velasco *et al*., "Secondary switched control with no communications for islanded microgrids," *IEEE Transactions on Industrial Electronics*, vol. 64, no.11, pp. 8534-8545, Nov. 2017.

[34] A. H. Alobaidi, S. S. Fazlhashemi, and M. Khodayar *et al*., "Distribution service restoration with renewable energy sources: a review," *IEEE Transactions on Sustainable Energy*, vol. 14, no. 2, pp. 1151-1168, Mar. 2023.

[35] M. Transsai, "Development of an object-oriented service restoration expert system with load variations," *IEEE Transactions on Power Systems*, vol. 23, no. 1, pp. 219-225, Jan. 2008.

[36] F. Shen, Q. Wu, and Y. Xue, "Review of service restoration for distribution networks," *Journal of Modern Power System and Clean Energy*, vol. 8, no. 1, pp. 1-14, Jan. 2020.

[37] F. Wang, C. Chen, and C. Li *et al*., "A multi-stage restoration method for medium-voltage distribution system with DGs," *IEEE Transactions on Smart Grid*, vol. 8, no. 6, pp. 2627-2636, Nov. 2017.

[38] E. G. Carrano, G. P. D. Da Silva, and E. P. Cardoso *et al*., "Subpermutation-based evolutionary multiobjective algorithm for load restoration in power distribution networks," *IEEE Transactions on Evolutionary Computation*, vol. 20, no. 4, pp. 546-562, Aug. 2016.

[39] B. Chen, Z. Ye, and C. Chen *et al.*, "Toward a MILP modeling framework for distribution system restoration," *IEEE Transactions on Power Systems*, vol. 34, no. 3, pp. 1749-1760, May 2019.

[40] J. Li, C. Zhang, and Z. Xu *et al*., "Distributed transactive energy trading framework in distribution networks," *IEEE Transactions on Power Systems*, vol. 33, no. 6, pp. 7215-7227, Nov. 2018.

[41] H. Ji, C. Wang, and P. Li *et al.*, "Robust operation of soft open points in active DNs with high penetration of photovoltaic integration," *IEEE Transactions on Sustainable Energy*, vol. 10, no. 1, pp. 280-289, Jan. 2019.

[42] A. Castillo, P. Lipka, J. Watson, *et al*., "A successive linear programming approach to solving the iv-acopf," *IEEE Transactions on Power Systems*, vol. 31, no. 4, pp. 2752-2763, Jul. 2016.

[43] L.Gan, N. Li, and U. Transopcu *et al*., "Exact convex relaxation of optimal power flow in radial networks," *IEEE Transactions on Automatic Control*, vol. 60, no. 1, pp. 72-87, Jan. 2015.